Limnol. Oceanogr., 56(1), 2011, 17–36

doi:10.4319/lo.2011.56.1.0017

Diel cycles of the particulate beam attenuation coefficient under varying trophic conditions in the northwestern Mediterranean Sea: Observations and modeling

Pierre Gernez,[a,b,1,*] David Antoine,[b] and Yannick Huot[b,2]

[a] ACRI-st, Sophia Antipolis, France

[b] Laboratoire d'Océanographie de Villefranche, Centre National de la Recherche Scientifique, Institut National des Sciences de l'Univers, Université Pierre et Marie Curie, Villefranche sur mer, France

Abstract

The changes in shape, amplitude, and timing in the diel variability of the particulate beam attenuation coefficient (c_p) were investigated at 4 and 9 m during two seasonal cycles at an oceanic site in the northwestern Mediterranean Sea under contrasting physical and trophic situations. We observed a diel cycle in c_p during the winter mixing of the water column, the development of the spring phytoplankton bloom, its collapse, and during the summer oligotrophy. The relative amplitude of the c_p diel cycle was about 10–20% during winter mixing and summer oligotrophy and at least twice as large during the spring bloom. Diel c_p minima generally occurred around sunrise and maxima a few hours before sunset. The specific particle rate of variation (r) was consistent over the diel cycle, with positive and negative values during daytime and nighttime, respectively. A striking feature of the r diel cycle was a morning maximum, i.e., before solar noon, which was successfully reproduced by a new model of particle assemblage growth rate based on three parameters: maximum growth rate, growth efficiency, and saturation irradiance. Each model parameter undergoes a diel cycle and shows a seasonal variation. A c_p-based estimation of the particle net community production is computed from the measurements and model outputs. Results compare favorably with modeled primary production on the basis of continuous measurements of surface chlorophyll using fluorescence.

The light-driven photosynthetic process provides the chemical energy requirement for most oceanic ecosystems. This process shows a clear diel cycle driven by the variability in solar radiation (Doty and Oguri 1957; Sournia 1974; Harding et al. 1981). The measurement, description, and quantification of the primary and accompanying secondary productions in oceanic environments has long been and remains a central theme of biological oceanography (Ryther and Yentsh 1957). Observation of a similar diel cycle in the particulate beam attenuation coefficient (c_p, Siegel et al. 1989) has provided an alternative and potentially powerful and nonintrusive method to address fundamental questions related to particle growth and production (Walsh et al. 1995; Marra 2002; Claustre et al. 2007). Yet observations of the diel cycle in c_p, usually made from ships, remain scant, of limited duration, and their interpretation difficult to generalize.

The particulate beam attenuation coefficient, c_p (m^{-1}), is an optical measure of the particle pool. It is the sum of the particulate scattering and absorption coefficients. When measured with a beam transmissiometer in the red part of the visible spectrum, where particulate absorption is only a small percentage of c_p, it is close to the scattering coefficient (Loisel and Morel 1998), which itself depends on the concentration, size, and nature of the particles. This measurement is nonintrusive, and is most sensitive to particles in the size range from $\sim$ 0.5 to 20 μm (Stramski and Kiefer 1991). A large variety of living organisms (autotrophs and heterotrophs) as well as nonliving particles (organic detritus and minerals) falls within this size range. It is now well established that c_p is a useful proxy for the measurement of particulate organic carbon (POC, mg m^{-3}) concentrations (Gardner et al. 1993, Loisel and Morel 1998; Claustre et al. 1999).

The measurement of c_p has become routine in the past decades, and repeated observations in the world oceans have revealed that the daily cycle in c_p is a nearly ubiquitous feature characterized by a diurnal increase and a nocturnal decrease. Observations of this cycle have been reported for instance from the Pacific Ocean (Cullen et al. 1992; Bishop et al. 1999; Claustre et al. 2007), the Atlantic Ocean (Stramska and Dickey 1992; Gardner et al. 1993; Marra 1997), the Arabian Sea (Gardner et al. 1999; Kinkade et al. 1999), and the Mediterranean Sea (Oubelkheir and Sciandra 2008).

The diurnal c_p increase has been related to photosynthetic organic production by phytoplankton (Siegel et al. 1989). Such an increase is expected as carbon accumulates within cells, leading to an increase in either the cell size or the cell refractive index or both (Stramski and Reynolds 1993). Beyond phytoplankton, other organisms very likely contribute to the daily variability in c_p. This is supported, for instance, by the observation of coincident maximum in the daily c_p variability and maximum of bacteriochlorophyll *a* concentration (Claustre et al. 2007) and heterotrophic bacteria abundance (Oubelkheir and Sciandra 2008).

* Corresponding author: pgernez@ucsd.edu

[1] Present addresses: Marine Physical Laboratory, Scripps Institution of Oceanography, University of California San Diego, La Jolla, California

[2] Université de Sherbrooke, Département de géomatique appliquée, Sherbrooke, Canada

The nocturnal decrease in c_p has been related to the decrease in cell size and refractive index via respiration and cell division (Stramski and Reynolds 1993). Diel processes are not restricted to growth and respiration and include grazing (Cullen et al. 1992), particle aggregation, and sinking. Moreover, rapid increases in the mixed-layer depth can redistribute the particle load and contribute to c_p variability (Gardner et al. 1995).

Laboratory studies have also shown diurnal changes in phytoplankton optical properties and c_p (Stramski and Reynolds 1993). Extrapolation of their results to the marine environment is never straightforward, however, because they are obtained using monospecific cultures under controlled conditions. The diurnal scale of the c_p variability has, therefore, also been investigated in situ from ships. In this case, the limitation comes from the inevitably small number of days during which repeated (e.g., hourly) measurements can be performed. It is difficult to extrapolate the results of such campaigns to the broad ocean or to the varied situations encountered on one site throughout the seasons. The development of instrumented moorings and autonomous profiling devices has increased the resolution and the duration of observations (Stramska and Dickey 1992; Bishop et al. 2002), and now provides new opportunities to assess the persistence of the diurnal cycles whatever the environmental conditions, as well as to characterize the diel variability over long periods.

A 2-yr (2006–2007) time series of near continuous (every 15 min) c_p measurements taken from a longer record of the Bouée pour l'acquisition de Séries Optiques à Long Terme (BOUSSOLE) optical buoy (Antoine et al. 2006) is analyzed here. The site is characterized by a seasonal cycle in the physical conditions, which results in seasonal changes in nutrient concentrations, particle abundance, size distribution, composition and optical properties (Marty et al. 2002; Antoine et al. 2006). On the basis of this unique data set, the first objective is to characterize the diel c_p variability under varying environmental conditions. Is a diel c_p cycle observed during each season and if so, how does the diel c_p cycle vary with the course of the seasons? The second objective is to estimate biogeochemical information about the mechanisms underlying the c_p diel variability.

The paper is organized as follows. The overall c_p changes over the years 2006 and 2007 are presented to describe the background of the observed area. Representative examples of the diel variability are presented at different seasons. The diel c_p variability is examined separately for each season. A model is then proposed to interpret the observations.

Methods

BOUSSOLE site and measurement platform—The study site is located in the northwestern Mediterranean Sea, about 32 nautical miles from the coast (Fig. 1). It is named BOUSSOLE, which is an acronym that literally translates from French as "buoy for the acquisition of a long-term optical time series." Although all important information about the site characteristics, the measurement platforms, and the instrumentation can be found in Antoine et al. (2006), some elements are described here for completeness and when they specifically concern the present study.

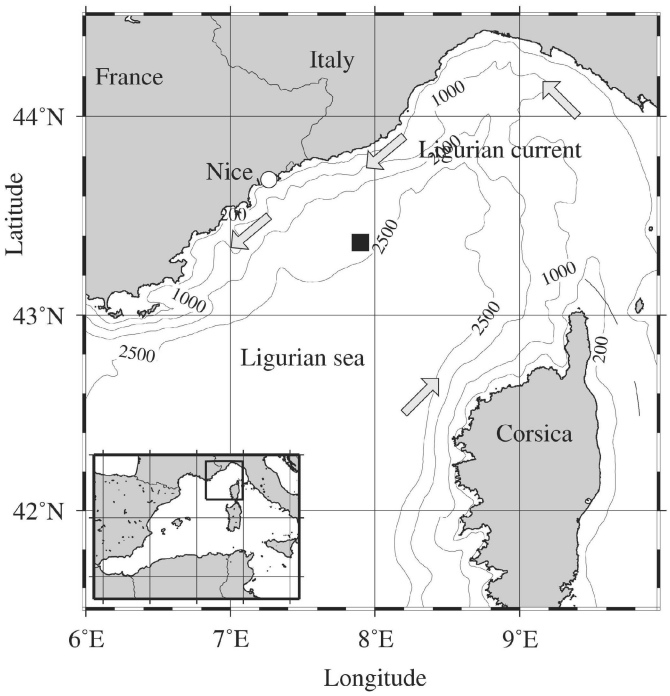

Fig. 1. The area of the northwestern Mediterranean Sea showing the southern coast of France, the island of Corsica, the main current branches (gray arrows), and the location of the BOUSSOLE buoy in the Ligurian Sea (black square).

The site is protected from coastal inputs by the Ligurian current that flows southwest along the coast (Millot 1999), so that waters permanently belong to the case 1 type (Antoine et al. 2008) following the Morel and Prieur (1977) definition. An important seasonality exists in physical conditions (D'Ortenzio et al. 2005), which drives the seasonal changes in phytoplankton composition and concentration. Oligotrophic conditions prevail during the summer with chlorophyll concentration lower than 0.1 mg m^{-3} (with minima around 0.05 mg m^{-3}). Higher concentrations up to about 3–5 mg m^{-3} occur during the spring phytoplankton bloom (February to March or April) when surface waters are nutrient replete. Moderate concentrations, between 0.1 and 0.3 mg m^{-3}, characterize most of the other periods of the year. There is accordingly a large range of optical properties at this site (Oubelkheir 2001; Antoine et al. 2006; Gernez 2009).

A buoy has been permanently deployed on this site since September 2003, and operates in a quasi-continuous mode with data acquisition every 15 min night and day. This platform has been specifically designed to optimize the measurement of radiometric quantities at two depths in the water column (nominally 4 and 9 m) and above the surface (Antoine et al. 2006, 2008), from which apparent optical properties (AOPs) are derived. Inherent optical properties (IOPs) are collected at the same frequency and the same depths. Two sister buoys equipped with the same sets of instruments are actually used, with rotation performed about every 6 months. This process allows one set of

instruments to be sent to the manufacturer and calibrated while the other set of instruments is at sea.

The site is visited monthly for buoy servicing, during which 0–400-m casts are performed for acquisition of hydrological data (conductivity, temperature and density, CTD), complementary IOPs and AOPs, and water sampling for subsequent phytoplankton pigment analyses and particulate absorption measurements.

More detailed information about the measurement protocols are provided below for the parameters specifically used in the present work. The buoy data (acquired every 15 min) used in this study are the beam attenuation coefficient c_p, the photosynthetically available radiation (PAR), the chlorophyll fluorescence (*FL*), water temperature, salinity, and density. The monthly cruise data used in this study are the phytoplankton pigment concentrations and mixed-layer depth (z_m).

Beam attenuation coefficient measurements—The beam attenuation coefficient at 660 nm $c(660)$ is measured every 15 min at the buoy collection depths (4 and 9 m) with 25-cm-path-length WETLabs® C-star transmissiometers. Acceptance angle is 1.2°. Effects of the acceptance angle on the measurement of beam c have been discussed in Boss et al. (2009). The instrument bodies are covered with copper tape. Source and detector windows are equipped with copper rings and are cleaned about every 2 weeks by divers using soft brushes. These measures have proven efficient in preventing biofouling. Corrupted data identified from the comparison of data collected before and after cleaning operations are eliminated and not used here. The particulate beam attenuation coefficient c_p is computed as $c - 0.364\ \mathrm{m}^{-1}$ (Bishop 1986). This is assuming that absorption, by dissolved organic matter in particular, is negligible at this wavelength (Bricaud et al. 1981).

A separate WETLabs transmissiometer is deployed monthly during the 0–400-m CTD casts. The deep c value (350–400-m average) is used as reference (Loisel and Morel 1998). The particulate beam attenuation is computed by subtracting this deep value from the total attenuation coefficient. To correct for any drift, the buoy c_p values have been forced to agree with the monthly cruise c_p values at the buoy collection depths. Occasional small offsets have been applied to the buoy c_p data.

Photosynthetically available radiation—The above-water downward irradiance E_s (W m^{-2} nm^{-1}) is measured at seven wavelengths (412, 442, 490, 510, 560, 665, and 683 nm) using a Satlantic OCI-200 series radiometer. It is used here to derive an approximate value of the above-water PAR([0+], μmol quanta m^{-2} s^{-1}), by discrete integration and extrapolation from these seven wavelengths between 400 and 700 nm:

$$\mathrm{PAR}(0^+) = 10^6 / (h v_0 N_A) \sum_{k=1}^{9} \lambda_k (E_s[\lambda_{k+1}] + E_s[\lambda_k])(\lambda_{k+1} - \lambda_k)/2, \quad (1)$$

where h, v_0, and N_A are, respectively, Planck's constant (6.626×10^{-34} J s), the speed of electromagnetic radiation in vacuo (2.9979×10^8 m s^{-1}) and Avogadro's number (6.022×10^{23} mol^{-1}). λ_k is taking value in (400, 412, 442, 490, 510, 560, 665, 683, and 700 nm). Note that the values of E_s at 400 and 700 nm are extrapolated using the variation from 412 to 442 nm and from 665 to 683 nm, respectively.

Phytoplankton pigments—Water sampling is performed during the cruises between the surface and a depth of 200 m. Only the data obtained from samples taken at 10 m are used here. Particles are collected onto 25-mm Whatman glass-fiber filters GF/F and then stored in liquid nitrogen. Algae pigment concentrations are measured in the laboratory using high-performance liquid chromatography (HPLC) following Ras et al. (2008). The total chlorophyll *a* concentration [TChl*a*] (mg m^{-3}) is computed as the sum of the concentrations of Chl a, chlorophyllide *a*, plus divinyl chlorophyll *a*. The relative proportion of picophytoplankton (< 2 μm), nanophytoplankton (2–20 μm), and microphytoplankton (20–200 μm) are determined from the concentration of phytoplankton pigments that have a taxonomic significance and can be associated with a size class, as described in Uitz et al. (2006).

Chlorophyll fluorescence—The stimulated chlorophyll fluorescence (*FL*, relative units) is measured on the buoy using a WETLabs FLNTUS fluorometer sensor also installed at ~ 9-m depth. To avoid the midday depression of *FL* caused by nonphotochemical quenching (Kiefer 1973), daytime *FL* values have been determined by linear interpolation between dusk and dawn measurements (example shown in Fig. 2A). The *FL* values are converted into equivalent chlorophyll concentrations [Chl] using the HPLC-determined [TChl*a*], using a power model (r^2 = 0.90, and root mean square = 0.12). The fit between coincident [TChl*a*] and fluorescence measurements is shown in Fig. 2B.

As the fluorescence measurements are affected by nonphotochemical quenching (*see* one typical example in Fig. 2), the variations of *FL* cannot be used to study the diel cycles of chlorophyll concentration. Only nocturnal (± 2 h around midnight) average values of [Chl] are used in the present study.

Ancillary physical information—The salinity (S), water temperature (T, °C), and the buoy depth (z_{buoy}, m) are measured with a Seabird SBE 37 SI CTD nominally installed at 9 m. The sea surface temperature (SST, °C) and the wind speed (U, m s^{-1}) are measured every hour by a weather buoy moored two nautical miles away from BOUSSOLE, operated and provided by the French weather forecast service, Meteo France. During the cruises, vertical T and S profiles are performed using a Seabird SBE 911 plus CTD equipped with sensors for pressure (Digiquartz Paroscientific), temperature (SBE 3), and conductivity (SBE 4). After determination of the density, two mixed-layer depths (respectively, z_m and z_{m2}) are computed using a density gradient criterion of, respectively, 0.125 kg m^{-3} and 0.03 kg m^{-3}: z_m is used to assess the

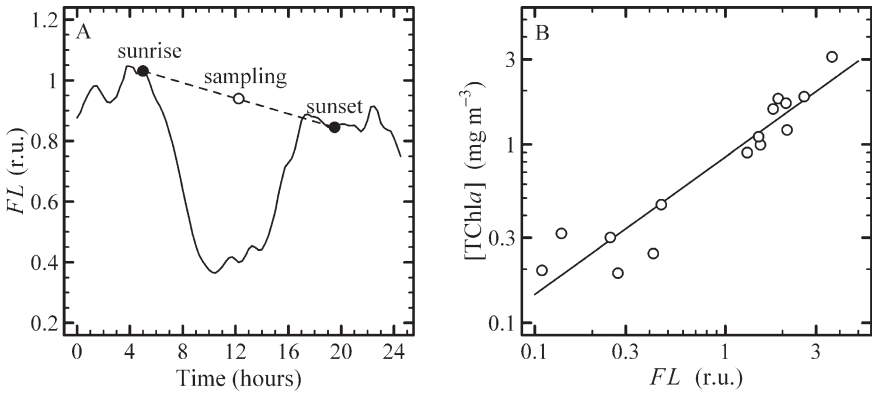

Fig. 2. (A) Schematic drawing illustrating how the value of fluorescence concomitant with the time of discrete water sampling is determined by linear interpolation between the sunrise and sunset values. (B) Relationship between [TChl*a*] and concomitant *FL* values, used to calibrate the fluorescence into equivalent chlorophyll concentration. r.u., relative units.

seasonal changes in mixed-layer depth, whereas z_{m2} is used to estimate the diurnal mixed-layer depth (Gardner et al. 1999). Daily values of mixed-layer depths are interpolated from the monthly estimations.

Average light for the particles transported within the mixed layer—Recent observations showed that particles can be mixed as deep as the bottom of the mixed-layer depth within 24 h (D'Asaro 2008). To estimate the light received by the particles as they travel throughout the mixed layer during a day, the mixed-layer averaged PAR ($\overline{\mathrm{PAR}}$) is computed from PAR(0^+) from the surface down to z_{m2} as in Babin et al. (1996, their eq. 9). In winter z_{m2} reached 70 m in 2007 and 400 m in 2006 during the exceptional mixing event (*see* later). z_{m2} is $\sim$ 10 m the rest of the year.

Data selection—To study the optical variations that result primarily from the ecosystem functioning, changes due to other possible causes (e.g., advection, mixing with water masses of different optical properties) have to be identified and eliminated from the analysis. The measurements used here are taken from a buoy, i.e., from a fixed geographical position, and the design of this buoy usually ensures that the measurement depths are maintained close to their nominal values of 4 and 9 m (Antoine et al. 2008). When the surface current occasionally becomes significant (it is usually weak at this site), the buoy can be pulled down. Such events are identified using a depth threshold of 11 m, as measured by the CTD sensor nominally located at 9 m.

Identification of water mass advection or of mixing of surface waters with deeper layers has been performed through parallel examination of the time series of c_p with T, S, SST, z_{buoy}, and U. The objective is to eliminate periods during which a large variability of T, S, and SST indicates unstable physical conditions during which the biologically driven diurnal cycle is likely to be masked and, therefore, significantly perturbed in amplitude or shape. An illustration is provided here on Fig. 3 for the time period from 13 July to 12 August 2006. The perturbation here identified between 21 July and 04 August is typical of summer, when a transient shallow ($\sim$ 10 m) and steep thermocline develops, with a decrease of several degrees within 2–3 m. When this thermocline oscillates because of internal waves, the temperature sensor installed at a nominal depth of 9 m experiences large temperature and salinity changes (up to 4°C and 0.5, respectively), whereas the SST is much more stable (diurnal change of 0.5°C to 1°C). The transmissiometer is also installed on the lower buoy arm ($\sim$ 9 m), so that its measurements have to be discarded in such circumstances. This peculiar situation disappears when the shallow thermocline is destroyed after two windy days (01 and 03 Aug).

Other physical perturbations can be identified with the time series as illustrated in Fig. 3, among which is intrusion of low-salinity water parcels. This phenomenon has been previously observed at the BOUSSOLE site (Andersen et al. 2009), and these events might affect phytoplankton (Marty et al. 2008) as well as the bacterial activity (Mével et al. 2008). As a consequence, days with anomalous salinity levels have also been excluded. The initial data set includes 530 measurement days over the years 2006 and 2007, from which a subset of 348 d has been selected. From this quality-controlled data set, the characteristics of the diurnal variability are investigated using different parameters that are expressed below and are schematically represented in Fig. 4.

Characterization of the diel variability—The amplitude of the diurnal variation in c_p (in m^{-1}) is:

$$\Delta c_p = c_{p2} - c_{p1} \tag{2}$$

where c_{p1} and c_{p2} are the c_p values at sunrise and sunset ($\pm$ 30-min averaged values), respectively. Note that Δc_p is not necessarily the maximum diurnal change.

The relative variation from sunrise (in %) is defined by:

$$\tilde{\Delta} c_p(k) = 100\left(c_p[k]/c_{p1} - 1\right) \tag{3}$$

where k is a fraction of a day (i.e., 1/24). By convention, it is counted from dawn such that sunrise, noon, sunset, and the

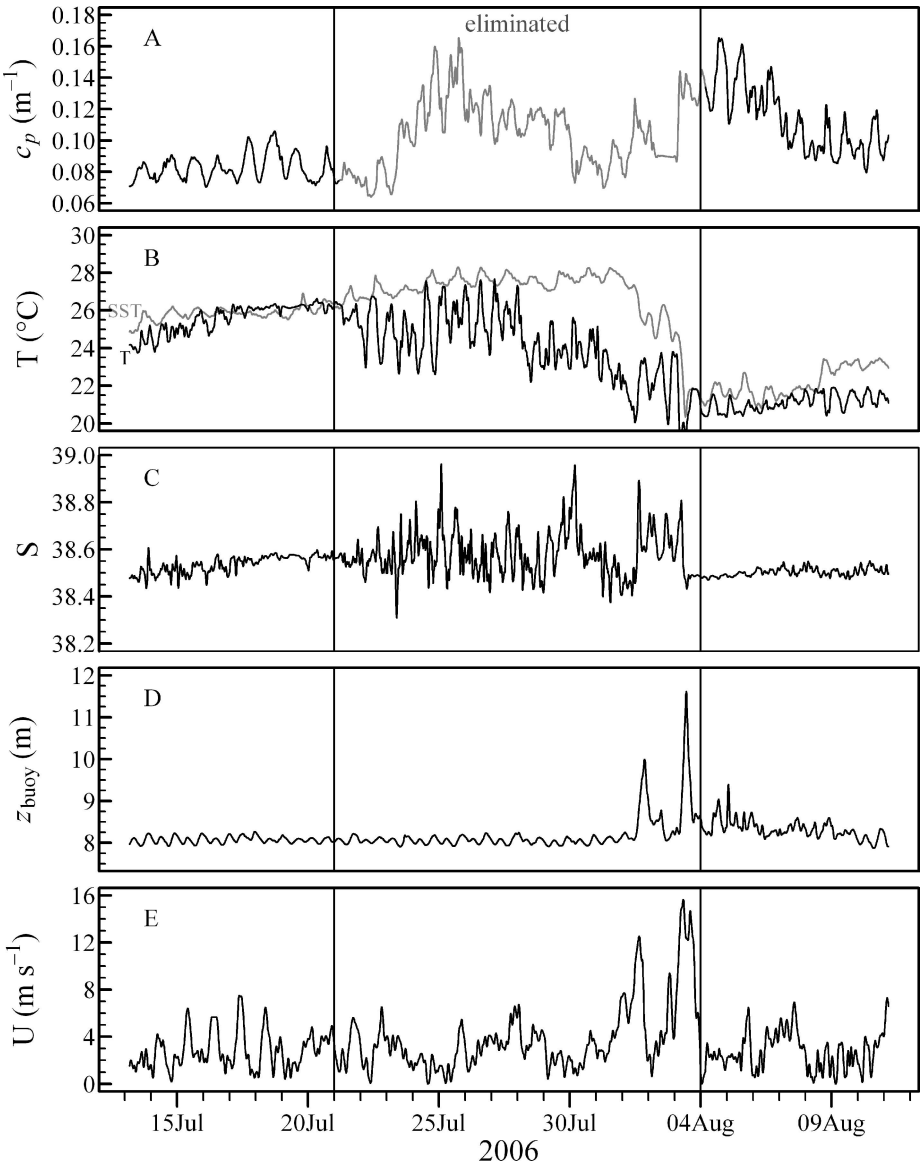

Fig. 3. (A–E) Time series of c_p, T, S, z_{buoy}, and U between 13 July and 12 August 2006 showing the period for which c_p data have been eliminated.

next sunrise correspond respectively to $k = 0$, 0.25, 0.5, and 1. Fractions of day are used rather than hours to allow comparison between days of varying photoperiod.

The instantaneous specific particle rate of variation (in d^{-1}) is computed as:

$$r(t) = \left(1/c_p\right)\delta c_p/\delta t \tag{4}$$

where δc_p is the variation within the time between two consecutive measurements (δt, 15 min). A 30-min running mean has been applied to $r(t)$ to smooth the data.

The diurnal rate of variation μ_{c_p} (in d^{-1}) is computed as the integral of r between sunrise and sunset, divided by 1 d to have units of d^{-1}:

$$\mu_{c_p} = (1/1\ \mathrm{d}) \int_{t=t_1}^{t=t_2} r\,(t)\,\mathrm{d}t \tag{5}$$

where t_1 and t_2 are respectively hours of sunrise and sunset. Equation 5 returns results that can be compared directly with Eq. 6 below, which has been used in previous studies (Cullen et al. 1992):

$$\mu_{c_p} = 24/(t_1 - t_2)\ln\left(c_{p2}/c_{p1}\right) \tag{6}$$

Results

Overall changes in c_p throughout two annual cycles—The 2-yr time series of daily averages of c_p and [Chl] is displayed in Fig. 5, along with the mixed-layer depth determined about once a month from vertical density profiles. The c_p variability is to the first order driven by a seasonal cycle, with values up to 0.8–1 m^{-1} during the spring phytoplankton blooms and of about 0.05–0.15 m^{-1} in summer and fall.

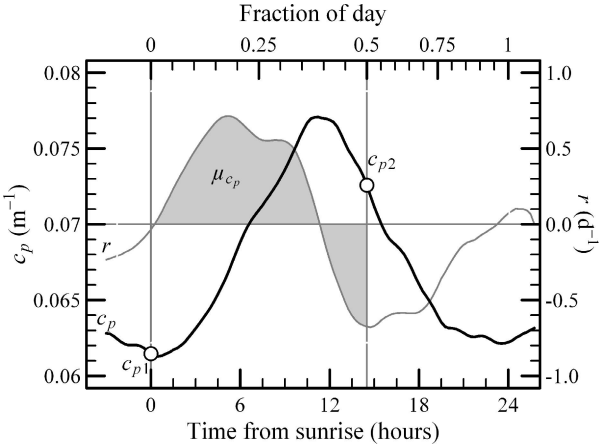

Fig. 4. Example of a diel cycle of c_p and r on 10 August 2007. The quantities μ_{cp}, c_{p1}, and c_{p2} are indicated to illustrate Eqs. 5 and 6. Sunrise and sunset are indicated by dashed vertical lines. The top axis represents fractions of the normalized day (i.e., sunset is 0.5 and midday is 0.25). In this case, note the longer step size during daytime compared with nighttime because day length is greater than 12 h.

A notable exception occurs in February–March 2006, with values as low as 0.015 m^{-1}, as a result of an exceptionally strong vertical mixing that diluted the particle population over a mixed layer z_m deeper than 2000 m. Extremely clear waters resulted from the vigorous mixing: diffuse attenuation for downward irradiance K_d as low as 0.024 m^{-1} at 490 nm, and a Secchi depth of 40 m were measured.

At the seasonal scale, the c_p variability is tied to that of [Chl], both experiencing changes by a factor of $\sim$ 50. However, as will be described later, changes in c_p do not systematically parallel those of [Chl]. Other changes also occur at smaller temporal scales, from day to day or within about a week.

Eventually, the diurnal variability represents another temporal scale at which significant variability occurs. It is represented in Fig. 5 by the shaded area made of all measured data points, behind the continuous black curve representing the daily average values. It is precisely this variability that will now be examined. Examples of diurnal cycles at four different seasons are described below, as a first step toward deriving average patterns of this variability as a function of the seasons. Their positions in the time series are identified on Fig. 5 by circled letters and a vertical line, and they are plotted in Fig. 6A–H under the form of 6-d time series extracted from the whole time series.

Examples of diurnal variability—Winter conditions: in March 2006 (Fig. 6A; 10–15 March, period A in Fig. 5), the water was exceptionally clear because of a vigorous mixing, and c_p varied between 0.017 and 0.024 m^{-1}. Although these values are extremely low, diel cycles occur with extrema at sunrise and sunset. The c_p variation experienced during a single day is as large as the change of the average daily values from the beginning to the end of the 6 d. The mean diurnal values of Δc_p and of μ_{cp} are 0.004 m^{-1} and 0.4 d^{-1}. In January 2007, when the mixed-layer depth was maximal that year (point E in Fig. 5), c_p is much higher, at 0.09 m^{-1} on average (Fig. 6E). Diel cycles are again observed. Their daily amplitude is greater than in 2006 ($\Delta c_p \sim 0.01$ m^{-1}) but the diurnal rate of variation is similar ($\mu_{cp} \sim 0.3$ d^{-1}).

During the spring phytoplankton bloom diel cycles are superimposed on a pronounced overall increase. Between

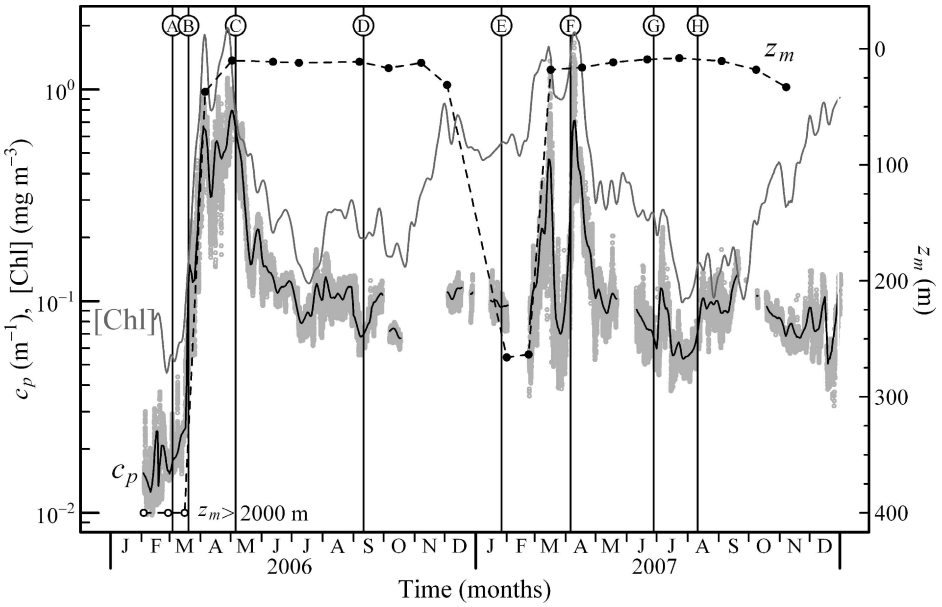

Fig. 5. Temporal variation of c_p (daily means in black thick line and instantaneous measurements in gray points), daily means of [Chl], and monthly cruise values of z_m. Note the exceptional mixing during winter 2006 where $z_m > 2000$ m. The positions of the examples displayed in Fig. 6 are indicated by circled letters.

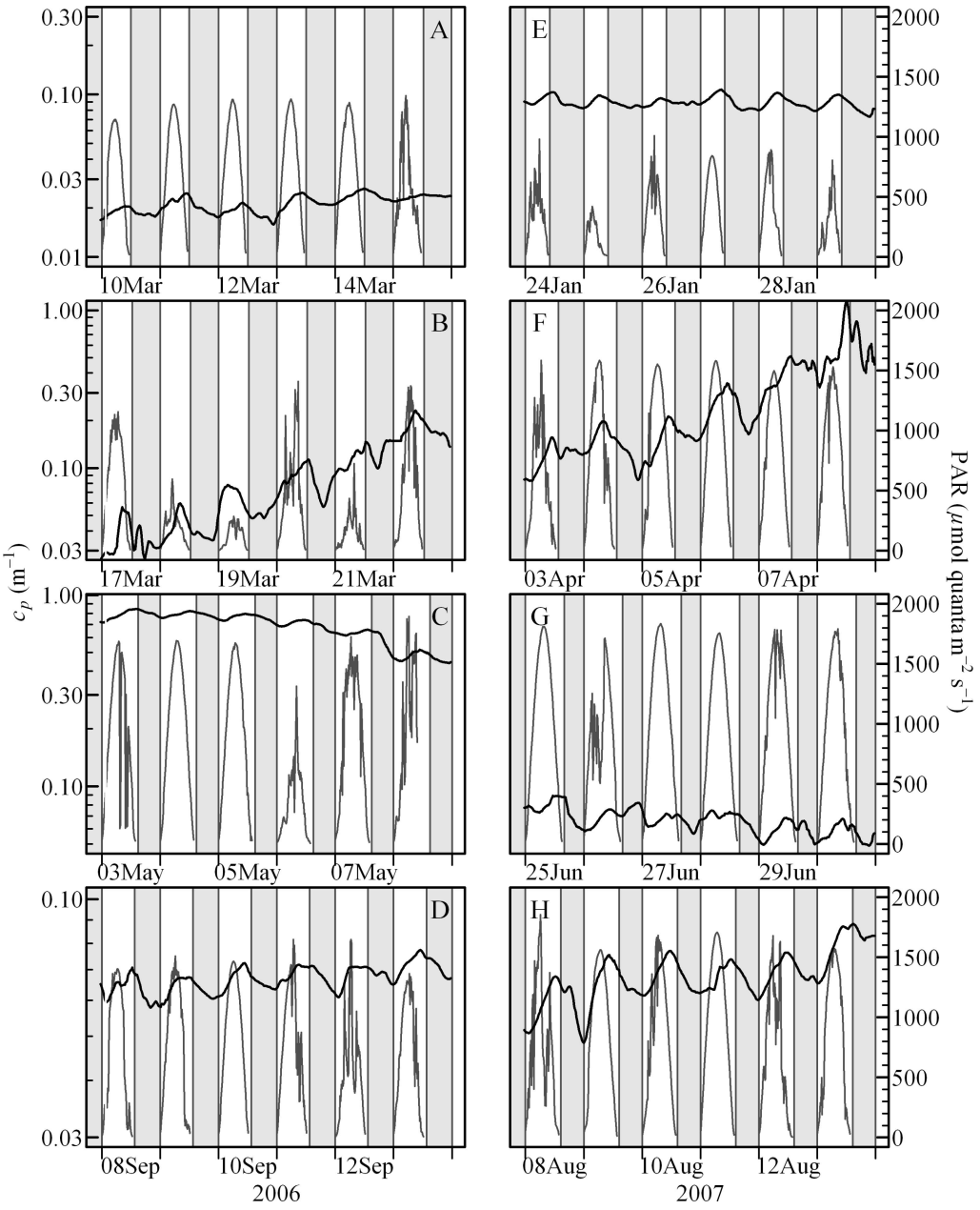

Fig. 6 (A–H). Example of 6-d time series of c_p and PAR(0+) for the time intervals indicated in Fig. 5. Gray bars indicate nighttime. Note the different scales on the left *y*-axis.

17 and 22 March 2006 (Fig. 6B), c_p increases by a factor of five, from 0.03 to 0.15 m^{-1}. Despite irregular diurnal variations likely due to the irregular PAR (intermittent clouds), a diel cycle emerges, with Δc_p between 0.02 and 0.1 m^{-1} and μ_{cp} between 0.7 and 1.3 d^{-1}. During the apogee of the bloom in 2007 (Fig. 6F; 3–8 April), c_p increases rapidly from 0.1 to 1 m^{-1}. As in 2006, the shape of the diel cycles is irregular, and the maximum is reached before sunset. The diurnal amplitude is large (up to 0.8 m^{-1}). The diurnal rate of variation is consistently high, between 0.5 and 2.5 d^{-1}.

The bloom declines after the upper layers are nutrient depleted. During the bloom collapse in 2006, c_p decreases by a factor of 2, from 0.8 to 0.4 m^{-1} (Fig. 6C; 03–08 May). Diel cycles are observed with mean Δc_p and μ_{cp} around 0.07 m^{-1} and 0.2 d^{-1}, respectively. The shape of the cycles is quite regular. Once again, the maximum occurs a few hours before sunset. A similar pattern, e.g., diel cycles superimposed on a general decrease, is observed after the 2007 bloom (Fig. 6G; 25–30 June), with c_p decreasing from 0.09 to 0.05 m^{-1}, and a diurnal amplitude and a rate of variation of $\sim$ 0.01 m^{-1} and 0.3 d^{-1}, respectively.

Regular diel cycles are observed during the summer and fall oligotrophy (Fig. 6D, H). Between the 08 and 13 September 2006, c_p varies by 0.01 m^{-1} at the diel as well as the weekly scale. The diurnal rate of variation is about 0.27 d^{-1}. Between the 08 and 13 August 2007, c_p varies a little more, from 0.05 to 0.09 m^{-1}. Repeatable diel cycles

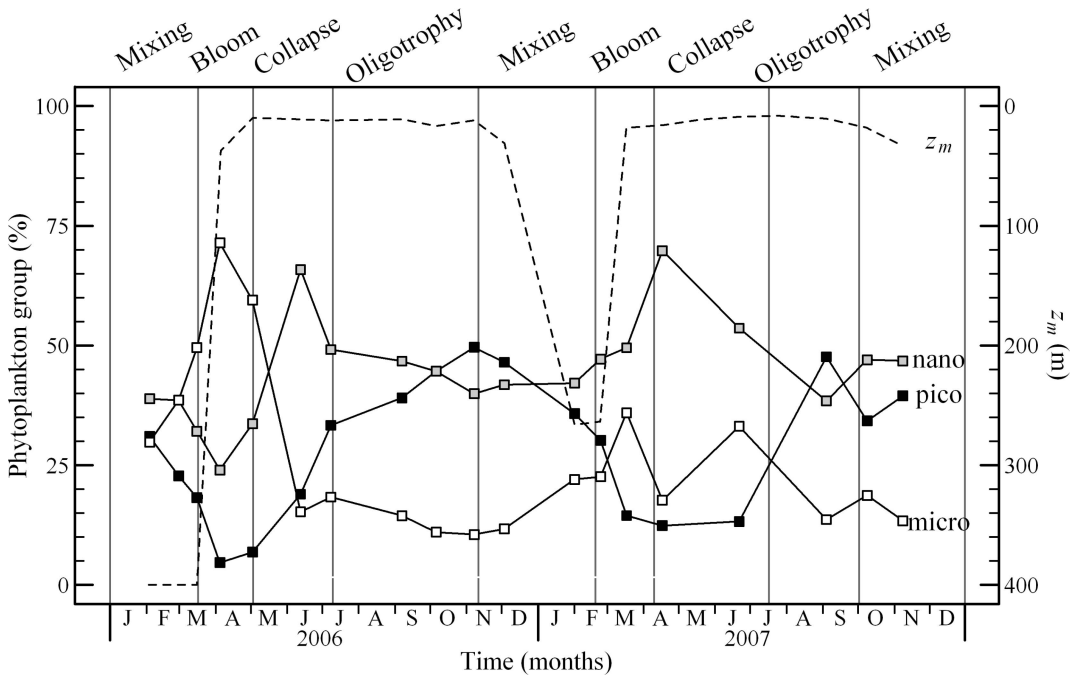

Fig. 7. Temporal evolution of monthly cruise values of z_m and of the proportion of pico-, nano-, and microphytoplankton from pigment signature obtained by HPLC. The segmentation in the four seasons defined in Table 1 is indicated.

occur, with maxima a couple of hours before sunset. Their diurnal amplitude and rate of variation are 0.015 m^{-1} and 0.45 d^{-1}, respectively.

In summary, a diel cycle (with diurnal increase and nocturnal decrease) appears to be a recurrent feature in the c_p signal at the BOUSSOLE site. Differences in the shape, amplitude, and rate of variation are observed at different periods of the years, which indicates that the trophic state has likely an influence on these parameters. To derive average figures (in terms of shape, amplitude, and rate of variation) for different seasons, the 2-yr time series is broken up into distinct segments. This is done with the objective of having segments with similar bio-optical characteristics and hence leading to smaller standard deviation around the average. The segmentation has been performed by examining the relationships between several bio-optical parameters, as described below.

Segmentation of the seasonal variations into distinct situations—It is known from previous studies that the seasonal cycle of the ecosystem at the BOUSSOLE site is typical of temperate and mid-latitude marine ecosystems (Marty et al. 2002). Consequently, four seasons, corresponding to situations of winter mixing, development of the vernal bloom, collapse of the bloom, and summer and fall oligotrophy, are differentiated. The term "season" is used, although the defined periods do not necessarily match the winter–spring–summer–fall calendar. The boundaries between the seasons have been adjusted to take into account the changes in the physical, trophic, and bio-optical conditions by examining the temporal variations of the mixed-layer depth z_m, the chlorophyll concentration [Chl], the phytoplankton pigment composition, and the c_p vs. [Chl] diagram.

The seasonal variations of z_m show two distinct regimes, with a period of mixing from December to February, a period of rapid decrease of the mixed-layer depth at the beginning of spring (around March–April), and a period of stratification the rest of the year, i.e., during summer and of the first half of fall (Fig. 5). Different physical conditions were experienced during the 2 yr examined here. Year 2006 is marked by an exceptional deep mixing in January–March ($z_m > 2000$ m). Such a deep mixing has not been observed in the past 15 yr (Marty et al. 2002). After April, the water column remains durably stratified during 7 months. In fall, the mixed layer starts to deepen. Year 2007 is marked by a shallower mixed-layer depth ($z_m < 400$ m) during winter. Stratification development starts earlier, in mid-February. Several strong wind events, from late March to early April, delayed the stabilization of the water column. The stratified period lasts from April to September, with a definitive breakdown in November. This description is based on monthly values determined over only a few days, which cannot represent rapid changes in z_m that may have occurred in between the monthly cruises.

The composition of the particle community is examined through the proportions of pico-, nano-, and microphytoplankton determined from diagnostic pigments (Fig. 7).

Microphytoplankton dominate the biomass (in terms of [Chl]) only during the bloom in 2006. Nanophytoplankton mostly dominate during the rest of the 2 yr, even during the bloom in 2007. After a minimum during the bloom, the proportion of picophytoplankton increases progressively from the bloom collapse to the end of oligotrophy. A maximum of about 50% is reached in October–November, where pico- and nanophytoplankton codominate. The dominance by picophytoplankton is not exceptional and

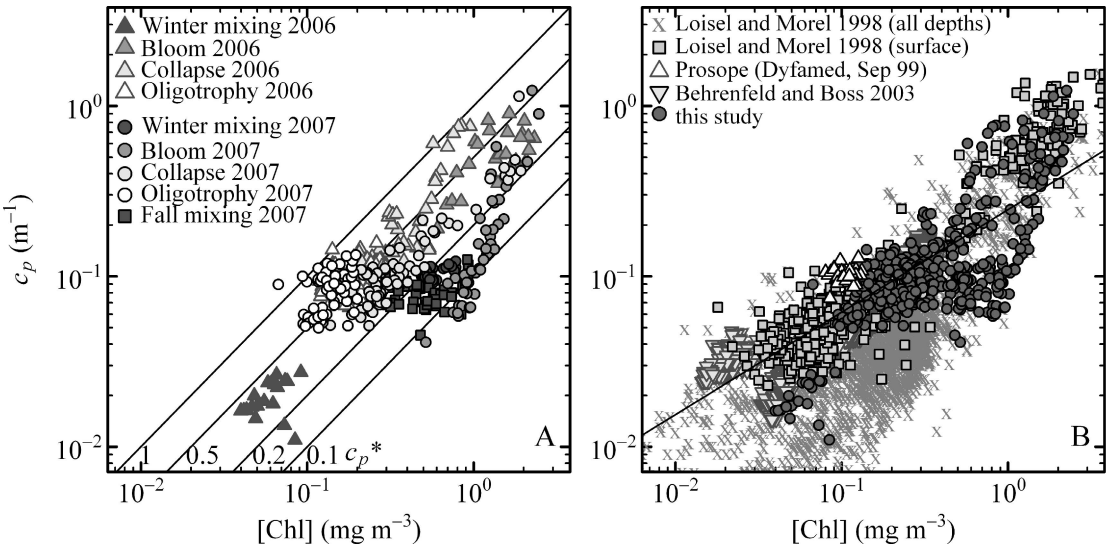

Fig. 8. (A) c_p vs. [Chl] for the different seasons defined in Table 1. Diagonal lines correspond to constant c_p* values. (B) c_p vs. [Chl] from the BOUSSOLE and other data sets (*see* legend). The black line is the relationship for surface waters from Loisel and Morel (1998, table 2, subset 2 + 3).

has also been observed at the end of summer in the 1990s and in 2000 and 2001 at or near this site (''Dynamique des flux atmosphériques en Méditerranée'' [DYFAMED] and BOUSSOLE data, not shown). The switch between nano- and microphytoplankton-dominated blooms is also a feature of this area: microphytoplankton dominated during the bloom of years 1994, 1996, 1997, 1999, 2000, and 2005 (DYFAMED and BOUSSOLE data, not shown), whereas the bloom was dominated by nanophytoplankton during the other years.

In 2007, [Chl] varies between 0.07 and 3 mg m^{-3} (Fig. 5). The [Chl] varies in parallel with c_p from February to mid-July. In October, the increase in [Chl] is not paralleled by a similar increase in c_p. As a result, the c_p vs. [Chl] diagram displays a specific pattern, with a △ shape (Fig. 8A). The right-hand-side segment of the △ corresponds to the bloom when c_p and [Chl] increase in parallel (gray symbols). The left-hand-side segment of the △ corresponds to the bloom collapse when c_p and [Chl] decrease in parallel (light gray symbols), yet follow another relationship during the bloom. The bottom-left extremity of the △ is completed during oligotrophy (white symbols), when [Chl] remains between 0.1 and 0.2 mg m^{-3}, whereas c_p varies between 0.05 and 0.15 m^{-1}. The closing horizontal segment of the △ corresponds to fall–winter mixing when c_p remains around 0.08 m^{-1}, whereas [Chl] increases from 0.3 to 0.9 mg m^{-3} (dark gray symbols). Correlation between c_p and [Chl] is observed during the development of bloom and its collapse, but with different relationships. Distinct clusters of points are observed during mixing and summer oligotrophy, which supports the segmentation into four seasons. It suggests that the natural variability of the c_p vs. [Chl] relationship is not random, but organized following a seasonal pattern. This reflects the seasonal changes in the optical properties of the particle assemblage, the pigment composition and packaging effect in phytoplankton community, and the variations between the respective proportions of algal and nonalgal particles (Loisel and Morel 1998), as well as the changes in carbon-to-chlorophyll ratio within phytoplankton cells. The c_p-to-[Chl] ratio, c_p*, is a convenient index to assess the changes in proportion between the algal and nonalgal compartments, as well as in the state of photoacclimation (Kitchen and Zaneveld 1990; Behrenfeld and Boss 2003). Low values of c_p* around 0.1 m^2 (mg [Chl])$^{-1}$ during the beginning of the bloom (Fig. 8A) suggest that first the c_p signal is dominated by phytoplankton and second the cells are photoadapted to low light, resulting in elevated cellular chlorophyll contents. During the last days of the bloom as well as during its collapse, c_p* is twice as large as during winter. An increase in the contribution of biodetritus, resulting from the end-of-bloom algal death and decay, probably partly explains the increase in c_p*. After the establishment of stratification, the particles remain trapped at the surface: a decrease in the intracellular chlorophyll concentration is expected, in response to the increase in irradiance levels experienced by algae. This may be accompanied as well by a high nonalgal particulate-to-phytoplankton ratio. During oligotrophy, c_p* exceeds 0.5 m^2 (mg [Chl])$^{-1}$, which is typical of surface oligotrophic situations (Loisel and Morel 1998).

Comparison with other data sets (Fig. 8B) shows that the c_p and [Chl] values are within the range of previously published results. The cluster of points observed during the oligotrophic seasons is consistent with previous observations made nearby the BOUSSOLE area in 1999 at the same time of the year (Oubelkheir et al. 2005) during the cruise ''Productivity of Oceanic Pelagic Systems'' (PROSOPE). The c_p vs. [Chl] relationships during collapse and oligotrophy are consistent with the global surface relationship from Loisel and Morel (1998). The bloom cluster, however, is located below their regression line and

Table 1. Definition of the seasons within which average parameters of the c_p diel cycles are determined. The dominant phytoplankton group is determined from the pigment composition after Uitz et al. (2006).

Season	Time intervals	Physical conditions	Dominant phytoplankton group	Number of days analyzed
Mixing	01 Jan–17 Mar 06 12 Nov 06–19 Feb 07 02 Oct–31 Dec 07	Mixing	Nanophytoplankton	86
Bloom*	18 Mar–3 May 06 20 Feb–10 Apr 07	Stratifying	Microphytoplankton	45
Collapse	04 May–10 Jul 06 11 Apr–17 Jul 07	Stratified	Nanophytoplankton	84
Oligotrophy	11 Jul–11 Nov 06 18 Jul–02 Oct 07	Stratified	Pico- and nanophytoplankton	133

* The definition of bloom is still controversial and a matter of debate (Behrenfeld 2010). The term bloom is used here to describe the seasonal increase in surface [Chl] occurring during the establishment of stratification (*see* Figs. 5, 7).

probably delimits a lower limit of the global data set (which includes deep measurements).

In summary, the data set has been segmented in four distinct seasons. Each season is characterized by different physical (i.e., mixing or stratification), trophic (i.e., high or low biomass), biogeochemical (i.e., domination of small or large phytoplankton), and bio-optical (i.e., position on the c_p-vs.-[Chl] diagram) conditions. The four seasons are described in Table 1.

The diurnal variability is now examined for each season. The following questions are addressed: Does a diel cycle occur? In this case, is there any difference in the amplitude, in the shape, or in the timing of the diel cycle?

Diurnal variability by season—The daily average normalized relative variability, $\tilde{\Delta}c_p$, is shown for each season (Fig. 9), along with the average daily variation of $\overline{\mathrm{PAR}}$. A diel cycle clearly appears whatever the season, even during the intense mixing of 2006 when midday $\overline{\mathrm{PAR}}$ is as low as 55 μmol quanta m^{-2} s^{-1}. The amplitude varies with the seasons: $\tilde{\Delta}c_p$ is between 10% and 20% during mixing, collapse, and oligotrophy and between 40% and 60% during the bloom. The standard deviation is of the same order as the mean, and is maximal during the bloom, when in fact $\tilde{\Delta}c_p$ exceeds 100% on some days. In contrast, the diel cycles are the most regular during oligotrophy. The timing is nearly the same at all seasons: c_p starts increasing at dawn and, except during the mixing of 2006 when c_p grows until dusk, c_p generally starts decreasing at 0.4 d (i.e., a few hours before sunset).

To compare the shapes of the cycles, the rate of variation is now examined by season (Fig. 10). The seasonal variation in the amplitude of the diel cycles is confirmed, with r reaching $\sim$ 0.6 d^{-1} during mixing, collapse, and oligotrophy and $\sim$ 1.6 d^{-1} during the bloom. Except for the 2006 winter mixing season where the maximum is later, the variation of the averaged r diel cycle generally presents the same feature: there is a sharp increase in the first half of the morning and the maximum is reached before noon (around 0.1 or 0.15 d). Then, r decreases slowly after midday and drops in late afternoon. Consistent with the maximum of c_p being reached before sunset, r becomes negative 0.1 d before sunset. Therefore, r does not strictly follow variations in $\overline{\mathrm{PAR}}$ but is generally positively skewed to the morning, with maximum a few hours before noon. Nighttime variations are usually small, with almost constant negative values until midnight and a slow recovery in the second half of the night.

The diurnal rate of variation μ_{cp} varies between -0.1 and 1.6 d^{-1}, and is not correlated with $\overline{\mathrm{PAR}}$ (Fig. 11): μ_{cp} is not higher during collapse and oligotrophy than during mixing, in spite of a fivefold increase in the mean $\overline{\mathrm{PAR}}$. Maxima occur during the bloom, with μ_{cp} around 1 d^{-1}. The rest of the year, μ_{cp} remains lower than 0.6 d^{-1}.

The variability of $\tilde{\Delta}c_p$, r, and μ_{cp} is similar in 2006 and 2007, which suggests that the seasonal variability is more important than the interannual variability. The winter of the first year had a much deeper mixed-layer depth than observed in the previous 15 yr, making the 2 yr very different physically. This vastly different preconditioning could be expected to cause lingering effects in the parameters mentioned above, but none is apparent despite average phytoplankton communities in the 2 yr.

Discussion

Estimation of the effects of the diurnal mixed-layer-depth dynamics on diel c_p *cycles*—As the main mixing or advection events have been removed by the data filtering on the basis of the salinity and temperature time series, the diel c_p cycles presented here are discussed in terms of biological activity only. This interpretation assumes that the diurnal changes in mixed layer do not significantly affect the diel c_p cycle. This is always the case during winter because the transmissiometers are far above z_m. During stratification, the mixed-layer diel cycle consists of a decrease from dawn to dusk, with stratification breaking at night (Gardner et al. 1999*b*). In this case, the influence of the diurnal change in z_m on the diel c_p cycle has been calculated from the monthly CTD casts, using z_{m1} and z_{m2} defined by a density gradient of respectively 0.125 and 0.03 kg m^{-3}. It is assumed that z_{m1} is constant over 24 h, whereas z_{m2} decreases during the day. At sunrise, z_{m2} is equal to z_{m1}. At the time of the cast, z_{m2} has decreased by a few meters. The mean difference between the 0-to-z_{m1} and 0-to-z_{m2} averaged c_p is 2% ($\pm$ 1.5%) and always smaller

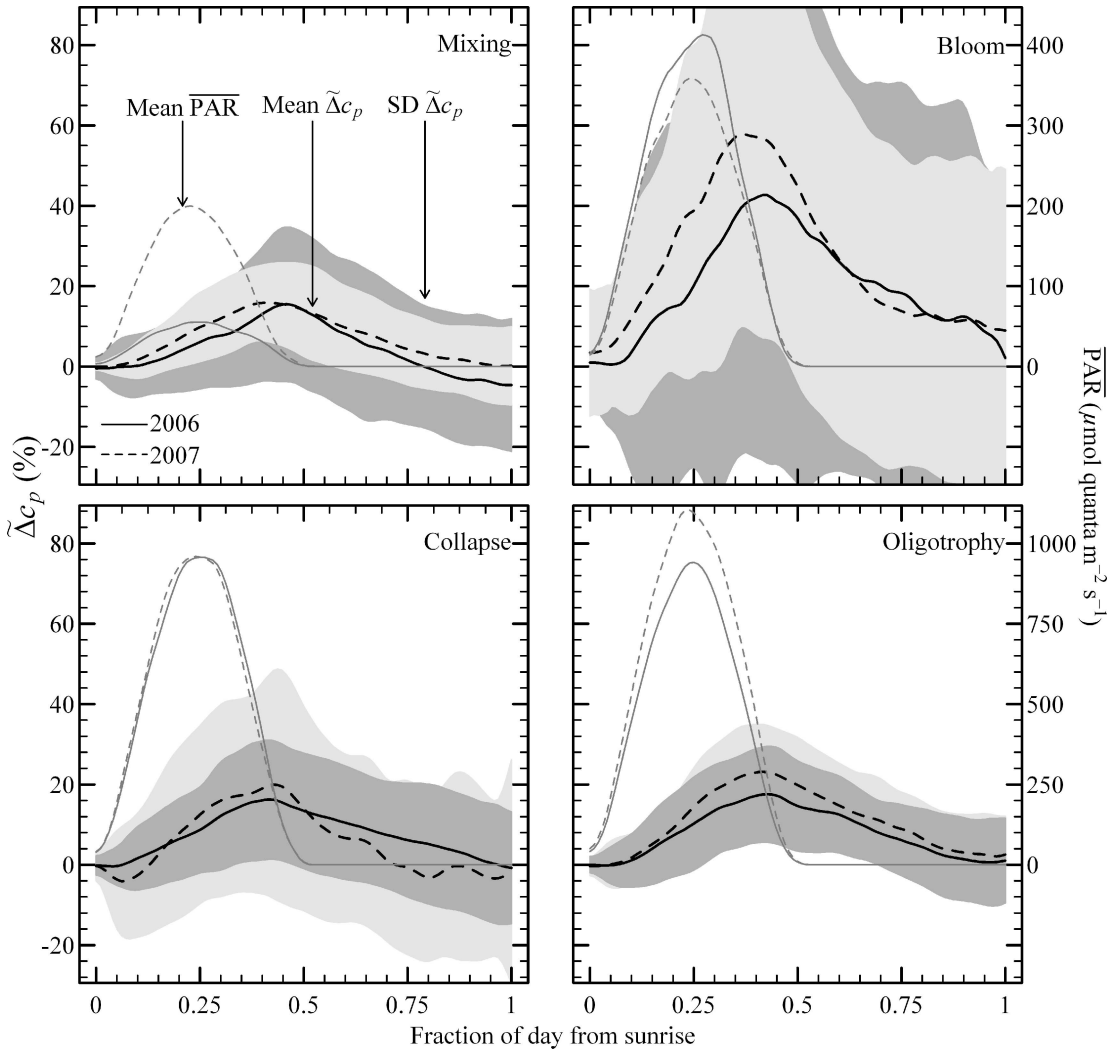

Fig. 9. Average $\tilde{\Delta}c_p$ (± standard deviation, SD) during situations of mixing, bloom, collapse, and oligotrophy in 2006 and 2007, as indicated. The average daily course of $\overline{\text{PAR}}$ is shown. Note that sunset is always at 0.5 d independent of seasons (*see* Fig. 4).

than 3% except on two occasions where it reached 6% and 12%. These exceptions occurred during the bloom, when the amplitude of the diel c_p cycle is at least 40%. The effect of diurnal variation in mixed-layer depth will not be considered in the rest of the discussion.

Diel cycles under contrasted seasons—Maximal values of $\tilde{\Delta}c_p$, r, and μ_{c_p} are observed during the bloom when the growth of the particle assemblage is not limited by light or nutrient variability (contrary to other seasons). Δc_p is important (> 40%). The values of μ_{c_p}, about 0.9 (± 0.6) d^{-1}, are consistent with results from previous studies performed under bloom conditions, for which μ_{c_p} was generally greater than 0.6 d^{-1} when [Chl] exceeded 0.3 mg m^{-1} (*see* Table 2 for a comparison with previously published results). The daily amplitude of the cycles is more important during the bloom of 2007 than of 2006. This might be related to differences in phytoplanktonic composition: in 2006, the bloom has been dominated by microphytoplankton, whereas nanophytoplankton dominated in 2007 (Fig. 7). This is consistent with laboratory experiments that suggest that $\tilde{\Delta}c_p$ is more elevated for monospecific cultures of pico- and nanophytoplankton than for cultures of microphytoplankton (Claustre et al. 2002).

$\tilde{\Delta}c_p$, r, and μ_{c_p} dramatically decrease as soon as the bloom is over and their minima occur during the bloom collapse and oligotrophy. The range of variation of μ_{c_p} (0.29 ± 0.16 d^{-1}) is consistent with the results of previous studies conducted in clear waters, with μ_{c_p} mainly in the range of 0.2 to 0.6 d^{-1} (*see* Table 2). The range of r variation (± 0.8 d^{-1}) compares well with the values (± 0.5 d^{-1}) observed by Siegel et al. (1989) in the oligotrophic equatorial Pacific ocean.

The low diel amplitude observed after the bloom is somewhat surprising. On one hand, one can expect that the amplitude of the diel cycle would have been greater during the oligotrophic summer because the day length is up to twice as long as during the winter mixing or the spring bloom. Moreover, small phytoplanktonic species, characterized in culture with a diurnal increase in attenuation cross-section up to 180% (Claustre et al. 2002), dominate the algal population after the collapse of the bloom. On the

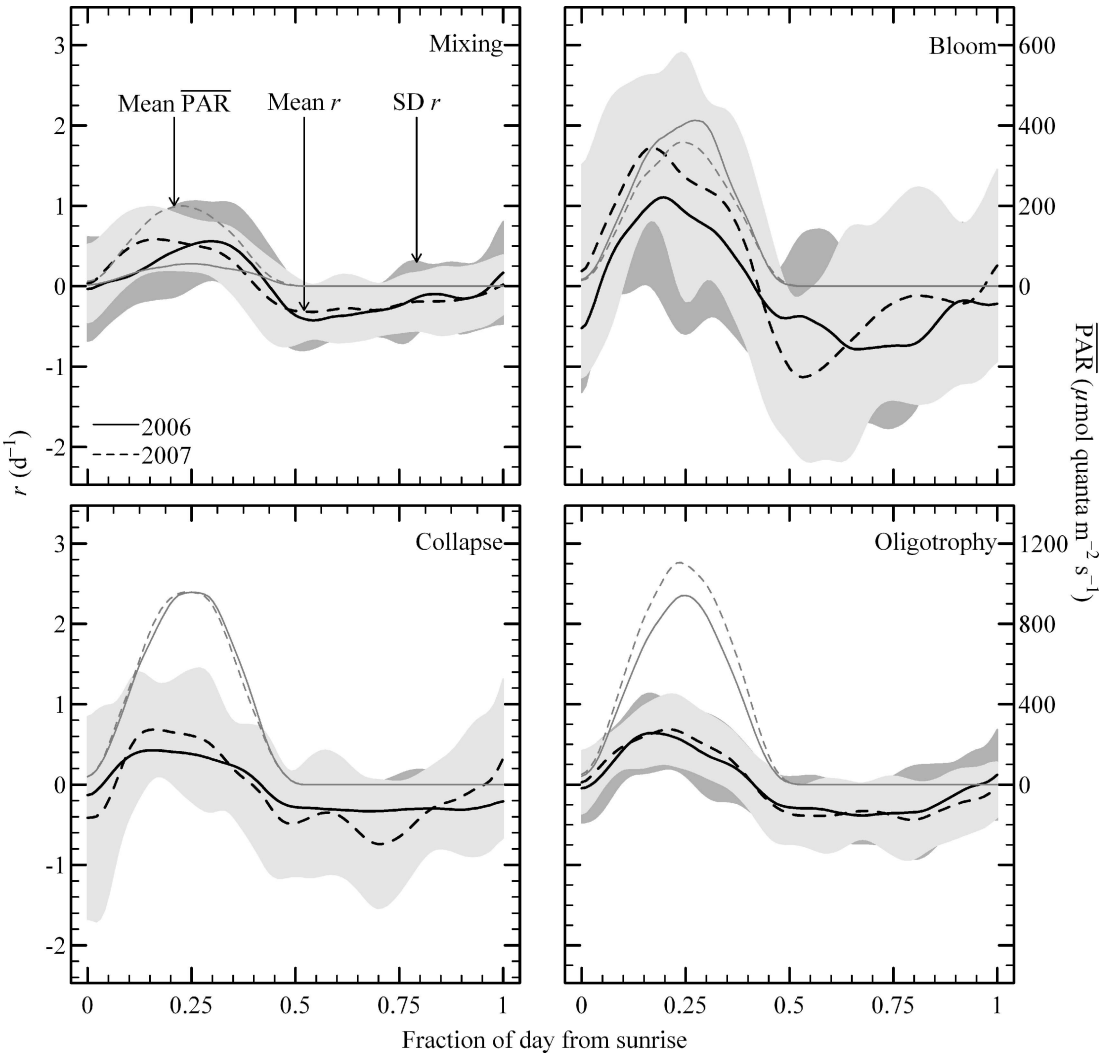

Fig. 10. As in Fig. 9, but for r.

other hand, there are several reasons that would explain the postbloom decrease in the daily c_p amplitude. First, estimated contribution of detrital particles to the total beam attenuation coefficient can reach 60% in summer at the BOUSSOLE site (Oubelkheir 2001). As detrital particles likely do not vary at the diel scale, an increase in their proportion diminishes the amplitude of the c_p diel cycle. Second, as phytoplankton are nutrient limited at this site in summer (Marty et al. 2002), a decrease in the photosynthesis (or at least in the cellular photosynthetic carbon accumulation) of the individual phytoplankters as well as a possible loss of the synchronization of the cellular division of the algal population is expected. Both factors tend to decrease the contribution of phytoplankton to the c_p diel cycle. Third, photosynthetic organisms are not the only living organisms responsible for the c_p variability. The role of heterotrophic organisms has been stressed at a hyperoligotrophic site of the South Pacific Ocean (Claustre et al. 2007) and it has been recently shown that heterotrophic bacteria are one of the main drivers of the c_p diel pattern in the oligotrophic Ionian Sea (Oubelkheir and Sciandra 2008). The contribution of bacteria to the diel c_p variability is not known: it could increase or decrease the amplitude of the cycles. In summer, nutrient-limited bacterial growth might also contribute to reduce the amplitude of the c_p diel cycles.

Timing of the r diel cycle—The shape of the diel r cycle differs from previous observations or models (Siegel et al. 1989; Cullen et al. 1992; Marra 1997). In previous studies, the rate of variation was assumed to be synchronous with $\overline{\text{PAR}}$. Results from the present study underline two deviations from this pattern (Fig. 10). First, r generally becomes negative 0.1 d (around 2–4 h) before sunset. Second, for all seasons except during the winter mixing of 2006, r reaches its maximum before noon. This morning maximum is consistent with the results of laboratory studies, where maximal increases in cell size, cell refractive index, carbon per cell, and bulk c_p all occurred early in the morning (Stramski and Reynolds 1993). This suggests that the variations of r observed here are driven by particle growth, with a maximum in the first half of the photoperiod.

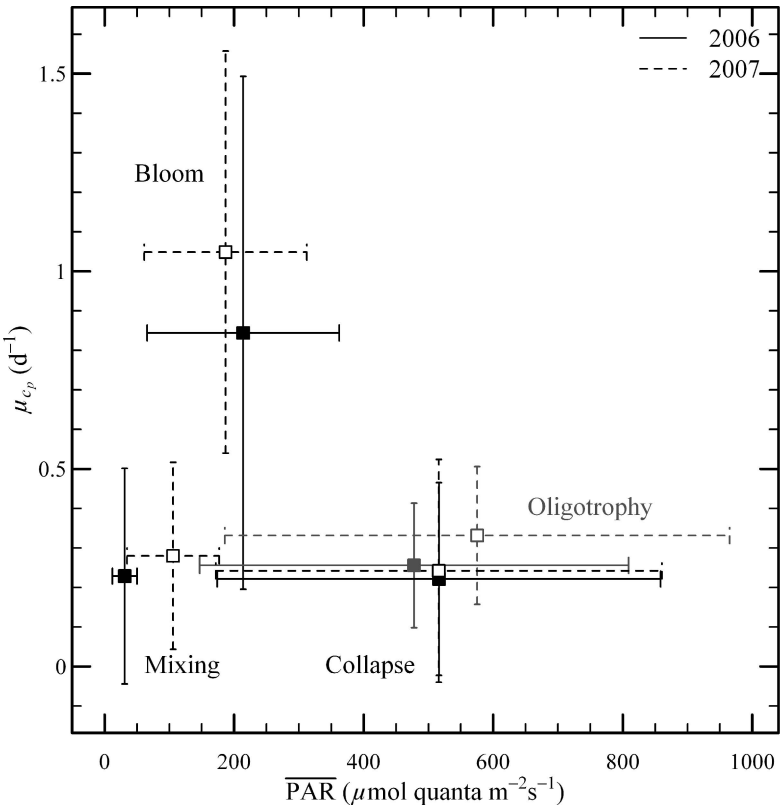

Fig. 11. Average and standard deviation of the μ_{cp} vs. $\overline{\mathrm{PAR}}$ diagram, for the four seasons in 2006 and 2007, as indicated.

Modeling r as a particle growth rate—A new model is now proposed to reproduce the variations of r, considered here as being a proxy of the particle assemblage growth rate. Indeed, theoretical considerations support the important role of particle growth in explaining c_p variability. The bulk beam attenuation coefficient of all particles present in a given water parcel is theoretically equal to (Morel and Bricaud 1986):

$$c_p = \int_{x=0}^{x=+\infty} N(x)\sigma_g(x)Q_c(x)\,\mathrm{d}x \tag{7}$$

where $N(x)$, $\sigma_g(x)$, and $Q_c(x)$ are, respectively, the particle size distribution, geometrical cross-section, and efficiency factor for attenuation of particles in the size range ($x - \mathrm{d}x/2$; $x + \mathrm{d}x/2$). Any change in the particle size strongly affects c_p because it modifies both σ_g and Q_c. Indeed, at a given wavelength (here 660 nm) and refractive index n, Q_c is a function of particle size. For n fixed between 1.035 and 1.06, Q_c increases linearly along a 1 : 1 slope for particles of equivalent diameter (D) smaller than 7–12 μm (Morel and Bricaud 1986), whereas Q_c remains almost constant when D exceeds 20 μm. As σ_g is proportional to D^2 and considering that the particles between $\sim$ 0.1 and 20 μm are the most efficient contributors to c_p (660 nm) (Stramski and Kiefer 1991), a daytime increase in particle diameter leads to an amplified increase in c_p by a power of 2 or 3. It is therefore likely that particle growth, by increasing D (and also n, as a result of carbon per cell accumulation), is the most important factor in shaping the c_p diurnal increase.

Model description—The lag observed between $\overline{\mathrm{PAR}}$ and r (Fig. 10) is similar to the lag between PAR and photosynthetic growth previously observed in cultures of diatoms (Harding et al. 1981; their fig. 4) and of *Prochlorococcus* (Bruyant et al. 2005; their fig. 8). It is proposed that the variation of r has the same origins: the growth parameters are varying during the day. It has indeed been known for many years that the photosynthetic activity of natural algal populations is not constant at the diel scale (Doty and Oguri 1957). The two parameters considered in the Bruyant et al. (2005) study were the maximum primary production rate per unit of biomass ($P^{\mathrm{B}}_{\mathrm{max}}$) and the initial slope of the production vs. irradiance curve, per unit of biomass (α^{B}). According to the observation of Bruyant et al. (2005), $P^{\mathrm{B}}_{\mathrm{max}}$ and α^{B} vary during the day, and the rate of carbon fixation is maximal in the morning. A new model for r is accordingly proposed. As in Siegel et al. (1989), r is the sum of a light-dependent growth term (r_{G}) and of a constant loss term (r_{L}). The loss term encompasses all factors contributing to the nighttime decrease (grazing by nocturnal migration, respiration, cell division, sinking, aggregation, nocturnal mixing) and is computed as the averaged value of r during night. The growth term encompasses the variation of all diurnally active particles. It is modeled similarly to that of a photosynthetic growth (Jassby and Platt 1976):

$$\hat{r}_{\mathrm{G}}(t) = r_{\mathrm{max}}(t)\tanh\left(\overline{\mathrm{PAR}}[t]/E_k[t]\right) \tag{8}$$

where r_{max} is the maximum rate of variation (equivalent to

Table 2. Diurnal specific particle variation rate (μ_{c_p}) in surface layers (0–30 m), as determined from the present study (using Eq. 5) and from previously published works (using Eq. 6 with c_p values as read on the indicated figure). Range of variability is indicated between brackets.

Reference	Location	μ_{c_p} (d^{-1})	Mean c_p (m^{-1})
Claustre et al. 2007, fig. 3	Equatorial Pacific	0.4	0.025
Claustre et al. 1999, figs. 10, 11	Equatorial Pacific	(0.4, 0.6)	(0.01, 0.08)
Siegel et al. 1989, fig. 2	Tropical Pacific	(0.15, 0.3)	0.07
Cullen et al. 1992, fig. 1	Equatorial Pacific	0.85	0.07
Oubelkheir and Sciandra 2008, fig. 3	Ionian Sea (Med.)	0.4	0.08
Durand and Olson 1996, fig. 6	Equatorial Pacific	1	0.15
Bishop et al. 1999, fig. 14	North Pacific	0.8	0.15
Stramska and Dickey 1992, fig. 9	North Atlantic	(0, 1)	0.16
Marra 1997, fig. 1, October	Sargasso Sea	0.14	0.21
Kinkade et al. 1999, fig. 4	Arabian Sea	0.35	0.22
Gardner et al. 1993, fig. 7a	North Atlantic	0.8	0.25
Marra 1997, fig. 1, March	Sargasso Sea	(0.6, 1.4)	(0.2, 0.4)
Stramska et al. 1995, fig. 9	North Atlantic	(0.3, 0.9)	(0.4, 0.7)
Present study:	Northwestern Mediterranean Sea	(−0.3, 1.8)	(0.01, 1)
Mixing		0.25±0.25	0.05±0.01
Bloom		0.90±0.60	0.60±0.30
Collapse		0.23±0.25	0.20±0.20
Oligotrophy		0.29±0.16	0.08±0.02

P^{B}_{max}), t is a fraction of day, $\overline{PAR}$ is the mixed-layer averaged photosynthetically available radiation, and E_k is the saturation irradiance. r_{max} is the product of the growth efficiency α (equivalent to α^{B}) and E_k:

$$r_{max}(t) = \alpha(t) E_k(t) \quad (9)$$

The daily variation of α and E_k has been parameterized after the fig. 4 in Bruyant et al. (2005):

$$E_k(t) = E_0 + E_1 \sin^3(\pi t/12) \quad (10)$$

and

$$\alpha(t) = \alpha_0 + \alpha_1 \sin^3(\pi[t + t_0]/12) \quad (11)$$

E_0 and α_0 are minimal values; α_1 and E_1 give the amplitude of variation. E_k is in phase with the irradiance, which is assumed to vary as a $\sin^3$ with time of day (Ikushima 1967), whereas α is in advance of t_0 with respect to $\overline{PAR}$. The value of the parameters α_0, α_1, E_0, E_1, and t_0 can be obtained by minimizing the difference $\hat{r}_G - r_G$ using a nonlinear least-squares method (box constraints quasi-Newton algorithm [Byrd et al. 1995; http://www.R.project.org]).

Comments of the results—An example of the diel variations of r_{max}, α, and E_k is shown when the model is applied to the averaged diel r cycle during the oligotrophy in 2006 (Fig. 12). The observed variation of r is well reproduced (Fig. 12A), which is consistent with two major assumptions: the beam attenuation particle specific growth rate is a function of irradiance, and the growth parameters vary at the diel scale.

The first assumption deserves a few comments. Although the first driver of the diel particle growth is likely phytoplankton, it is, however, suspected that small heterotrophs in the size range 0.1–10 μm (in particular heterotrophic bacteria) significantly contribute to the c_p diel cycle (Oubelkheir and Sciandra 2008). Recently, it has been shown that heterotrophic bacteria might explain about a third of the c_p spatial variability in oceanic regions (Montes-Hugo et al. 2009). A diel cycle in the activity of free-living bacteria has been previously observed in the Mediterranean Sea (Gasol et al. 1998; Mével et al. 2008) as well as in other locations (Fuhrman et al. 1985; Van Wambeke et al. 2009), but their synchronicity with phytoplankton is not a general rule. Yet, a tight coupling between the photosynthetic extracellular release of organic material and its consumption by bacteria has been observed in the northwestern Mediterranean Sea (Gasol et al. 1998; Mével et al. 2008). In the oligotrophic North Pacific Ocean, it has been observed that the rates of [^{3}H]leucine incorporation (i.e., bacteria growth) responded to irradiance in a photosynthesis-like manner (Church et al. 2004).

The second assumption (the existence of a diel cycle for the growth parameters r_{max}, α, and E_k) is clearly justified by previous observations (Doty and Oguri, 1957; Bruyant et al. 2005). It makes it possible to reproduce the asymmetry of r (Fig. 12A), which would have been impossible using constant values. The causes of the diel cycles in the growth parameters (e.g., photoinhibition or alternative electron sink) are, however, not explained here. The phasing of α and r_{max} (Fig. 12B) is consistent with results from Bruyant et al. (2005): α decreases until midday and r_{max} maximum generally occurs before irradiance is maximal. Over an average day during oligotrophy, α and r_{max} vary by a factor of 2 and 4, respectively. With $\overline{PAR}$ varying between 0 and 950 μmol quanta m^{-2} s^{-1}, E_k increases from 150 to 450 μmol quanta m^{-2} s^{-1} (i.e., from 15% to 50% of midday $\overline{PAR}$) as a result of photoadaptation. This is equivalent to the range of variation reported by Bruyant et al. (2005). At station ALOHA of the Hawaii Ocean Time-series, a

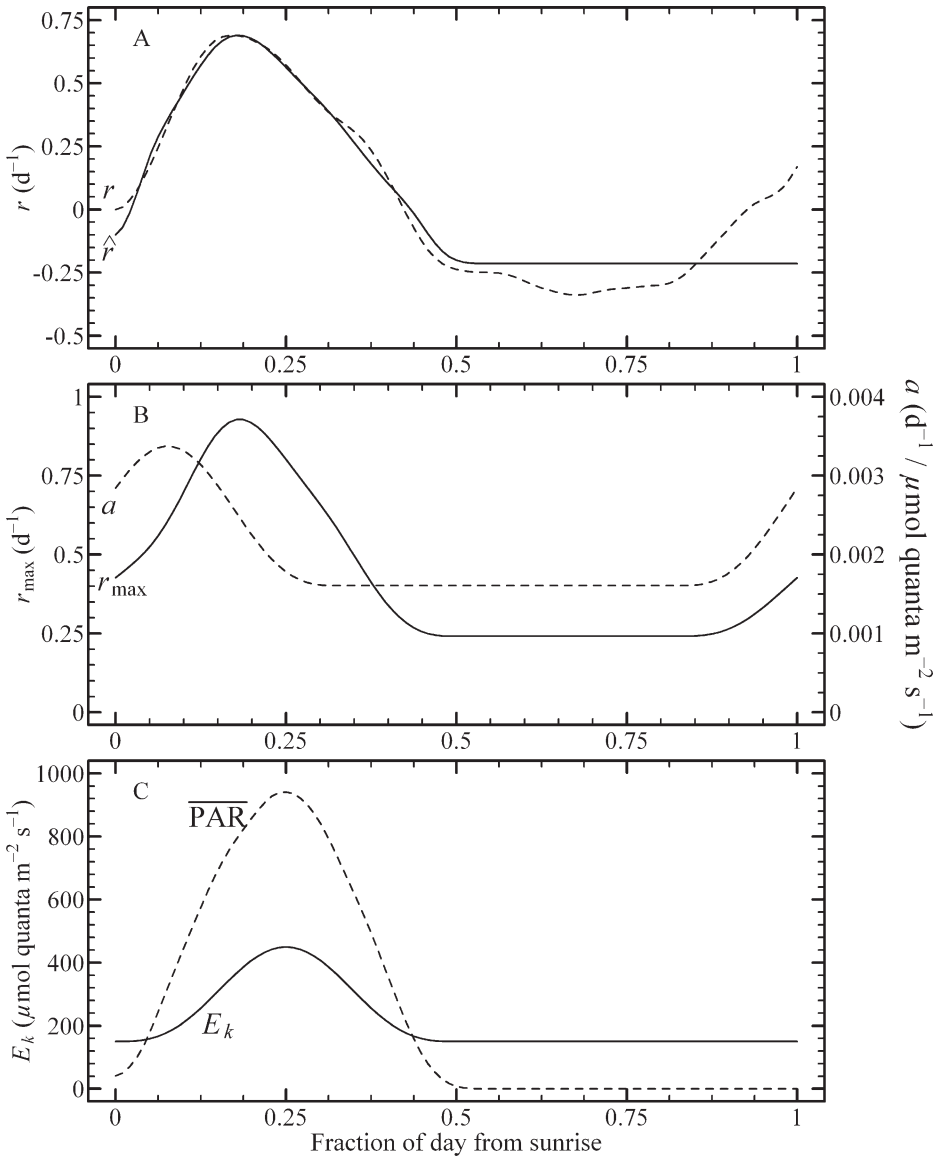

Fig. 12. During the oligotrophy in 2006, diel cycles of (A) averaged r and model output $\hat{r}$; (B) model outputs of r_{max} and α; (C) model output of E_k and averaged $\overline{PAR}$.

similar, threefold (in % of $\overline{PAR}$) diurnal increase in E_k has been observed (Ondrusek et al. 2001).

When applying our model to other seasons, the average maximum-to-minimum ratios of α, r_{max}, and E_k vary between 1.5 and 2.5, between 2.5 and 5, and between 2 and 4, respectively. Maximum α generally occurs just after sunrise, whereas r_{max} peaks later in the morning. Consistent with Bruyant et al. (2005), but contrary to other studies (Harding et al. 1981), the diel cycles of α and of r_{max} are not in phase, which is due to the fact that E_k is not constant during daytime (Fig. 12) in our model. E_k is always in phase with $\overline{PAR}$. At night E_k and r_{max} remain constant, whereas α starts to increase before sunrise. One exception occurs: during the mixing 2006, r_{max} and α present an afternoon maximum. Other studies have shown afternoon peaks in P^B_{max} (Malone 1971), but morning (Taguchi 1976) and midday maxima have also been frequently observed (Shimada 1958).

The seasonal variations of the parameters α, r_{max}, and E_k are shown in Fig. 13, where average values of the model parameters are plotted for each situation. The same trend is observed for α and r_{max}, with maxima during the bloom (Fig. 13A, B). The seasonal averages of α and r_{max} are correlated with [Chl], even if maxima in α and r_{max} also occur during the winter of 2006. Contrary to r_{max}, the seasonal variation of E_k is not related to the level of biomass. E_k increases regularly from winter to summer, in parallel with increasing $\overline{PAR}$ (Fig. 13C), likely as result of photoadaptation.

The time dependency at the diel scale of the growth parameters should be considered to improve the accuracy of predictive models of particle growth (Harding et al.

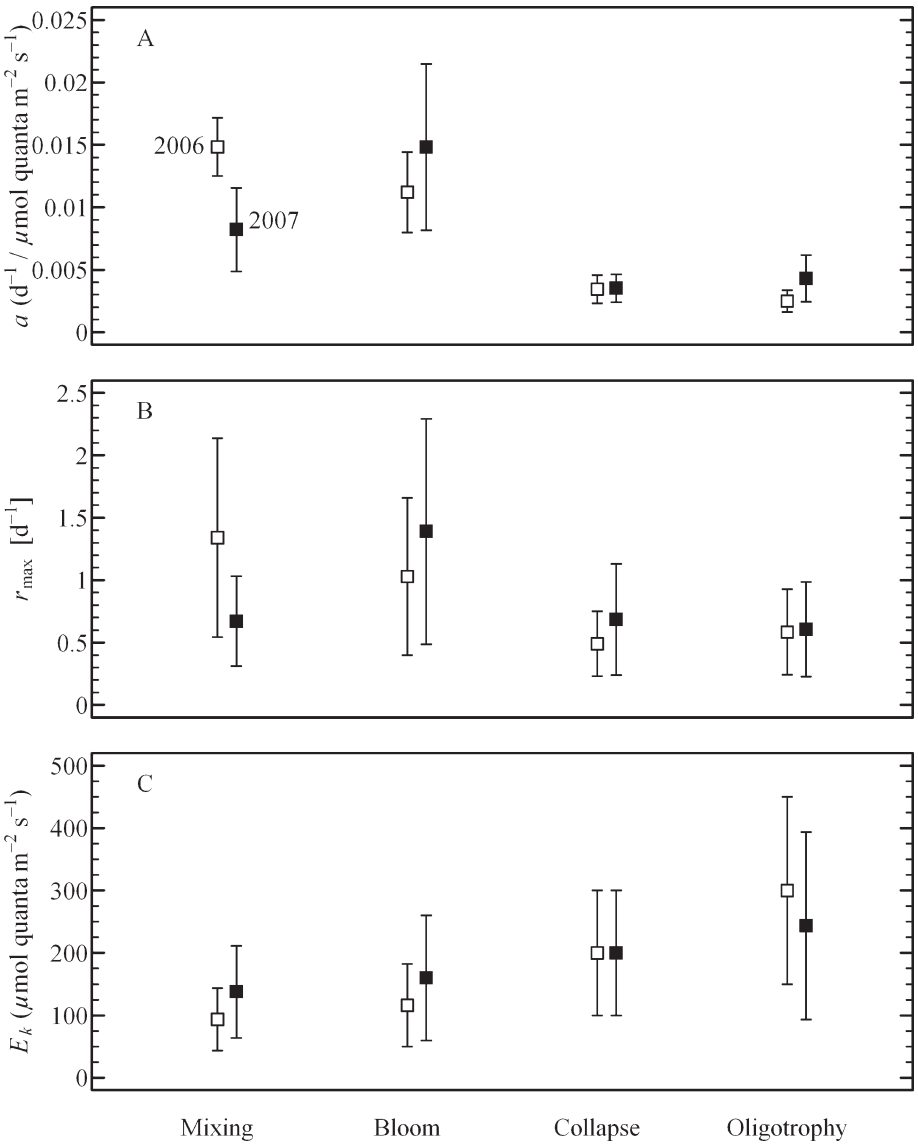

Fig. 13. (A–C) Seasonal variation of the mean parameters α, r_{max}, and E_k for 2006 and 2007 as indicated. The vertical bars are the differences between the minimum and maximum values over a day and do not represent error in the parameters.

1982). Taking into account the diel as well as the seasonal variation of the parameters α, r_{max}, and E_k, a tentative estimation of the organic matter production by photosynthetic and heterotrophic particulate growth is now proposed.

Application of the model: Estimation of the particulate net community production—From the measurements performed here, it is not possible to determine whether the daytime production of POC is caused by increase in the abundance, size, or carbon content of particles (or by a combination of all). Yet, it is possible to estimate a bulk, net increase in POC (ΔPOC) from the diurnal increase of c_p between sunrise and sunset (Siegel et al 1989; Claustre et al. 2007) using:

$$\Delta\mathrm{POC} = \Delta\left(c_p / c_c^*\right) \tag{12}$$

where c_c^* is the carbon-specific beam attenuation, i.e., the c_p-to-POC ratio. Different c_c^* have been reported for various phytoplankton species and nonalgal material, and the bulk c_c^* is dependent upon the particle community composition (Claustre et al. 2002). At the BOUSSOLE site, seasonal variability in the carbon-specific attenuation is expected, with lower values during oligotrophy and enhanced values during spring. The seasonal variation of c_c^* was not measured, but it should be less than its global geographical variability, which is about 20% (Gardner et al. 2006, their fig. 2). The carbon-specific attenuation may also vary during the day. Diel variation of 15% to 60% has been reported for various phytoplanktonic species in culture (*see* Claustre et al. 2002, their table 2) but it is likely that in situ diel variation in the bulk c_c^* is of lesser amplitude. A constant c_c^* of 1.78 m^2 (g C)$^{-1}$ (PROSOPE cruise, DYFAMED station, September 1999, Oubelkheir et

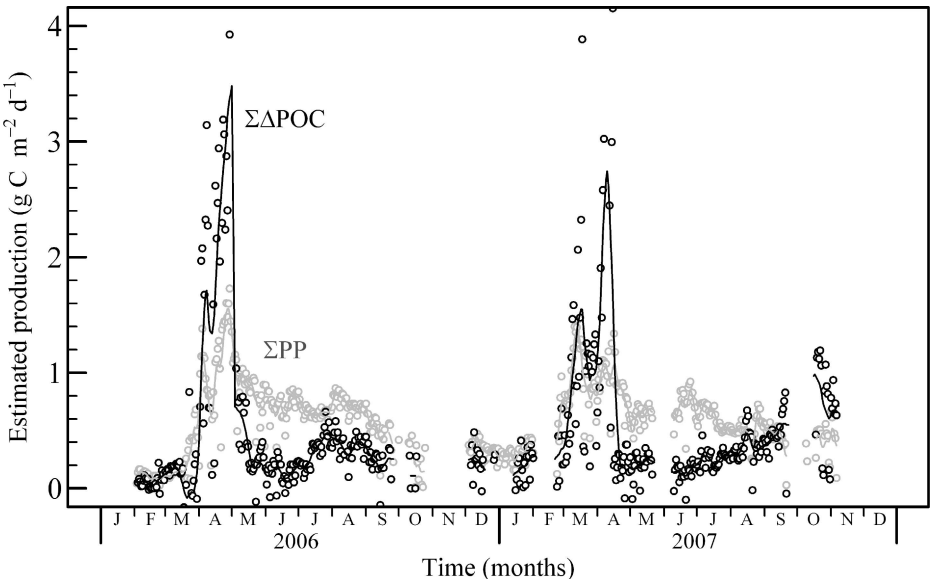

Fig. 14. Seasonal variation of ΣΔPOC and ΣPP. The points indicate daily values; the lines show a 3-d running mean.

al. 2005) is adopted here. ΔPOC is estimated from Δc_p using:

$$\Delta\mathrm{POC} \sim \Delta c_p / c_c * \tag{13}$$

The diurnal increase in c_p is then computed using:

$$\Delta c_p = \hat{c}_{p2} - c_{p1} \tag{14}$$

where c_{p1} is the sunrise value and $\hat{c}_{p2}$ is the sunset value modeled from c_{p1} using the model of r presented above. This model has five parameters (E_0, E_1, α_0, α_1, and t_0, *see* Eqs. 10, 11), for which different values have been computed at each season (mixing, bloom, collapse, or oligotrophy) and year (2006 or 2007). It has previously been reported that Δc_p is almost constant from the surface to the bottom of the euphotic zone (Siegel et al. 1989; Claustre et al. 2007). A column-integrated ΣΔPOC is computed from the surface value ($\Delta\mathrm{POC}_{\mathrm{surface}}$), following:

$$\Sigma\Delta\mathrm{POC} = Z_{eu} - \Delta\mathrm{POC}_{\mathrm{surface}} \tag{15}$$

ΣΔPOC shows a strong, 10-fold, seasonal variation (Fig. 14), with similar results in 2006 and 2007. The seasonal cycle is characterized by a maximum around 3 g C m^{-2} d^{-1} during the bloom, two minima of about 0.2 g C m^{-2} d^{-1} during mixing and collapse, and slightly more elevated values around 0.4 g C m^{-2} d^{-1} during oligotrophy.

In an attempt to validate the estimation of ΣΔPOC the results are compared with a standard light-photosynthesis model of primary production (Morel 1991). This model is typically used to estimate primary production from satellite ocean color [Chl] (Antoine and Morel 1996). It is applied here to the in situ surface [Chl] BOUSSOLE time series. Briefly, the computation of the primary production integrated over the euphotic zone (ΣPP) is based on the following global equation (Morel and Berthon 1989):

$$\Sigma\mathrm{PP} = 1/J_C < \mathrm{Chl} >_{\mathrm{tot}} \mathrm{PAR}\psi * \tag{16}$$

where $<\mathrm{Chl}>_{\mathrm{tot}}$ represents the column-integrated chlorophyll content (g Chl m^{-2}) determined form the surface [Chl], $\psi*$ is the cross-section of algae for photosynthesis per unit of areal chlorophyll biomass (m^2 [g Chl]$^{-1}$), and J_C is the energetic equivalent of photosynthetic assimilate (kJ [g C]$^{-1}$).

Two main significant differences are expected between ΣΔPOC and ΣPP. They do not represent the same biogeochemical processes: ΣΔPOC is an estimation of the particulate net community production, which includes heterotroph growth and losses (Claustre et al. 2007), whereas ΣPP is an estimate of the net primary production (Morel 1991), which concerns only autotrophs. The way ΣΔPOC is modeled takes into account the seasonal variability of the growth conditions because the set of parameters used to derive $r_{\max}$, α, and E_k depends on the season (*see* above). On the contrary, the parameters used in the standard algorithm of primary production are constant (Antoine and Morel 1996).

The variation of ΣPP (Fig. 14) is consistent with the average seasonal cycle reported in Marty and Chiaverini (2002) between 1993 and 1999 (their fig. 4). ΣPP shows the same seasonal pattern as ΣΔPOC but its magnitude is not as important. It shows lower values during the bloom and higher values in summer. During summer ΣΔPOC is lower than ΣPP, with a net negative difference up to 0.5 g C m^{-2} d^{-1}, but the differences vanish when the mixing starts. The most striking difference occurs during the bloom apogee, with a net positive difference of 1 to 2 g C m^{-2} d^{-1} and with ΣΔPOC three times higher than ΣPP. Interestingly, during the bloom, c_p increased from $\sim$ 0.1 to 1 m^{-1}, which is about three times more than [Chl], which increased only from $\sim$ 1 to 3 mg m^{-3} (Fig. 8). The difference between

ΣΔPOC and ΣPP during the bloom might therefore be due to the factor of three between the increase rate of c_p and the increase rate of [Chl].

This study demonstrates that in situ high-frequency transmissiometer measurements can offer more than the sole beam attenuation coefficient. The rate of c_p variation could be used to investigate the growth rate and the carbon accumulation of the particle assemblage. However, although this interpretation appears correct, it remains difficult to know exactly what part of the assemblage is represented by the measurement. Improving the certainty and accuracy of c_p-based bulk estimates ideally requires concomitant sampling of particle composition, size distribution, and organic carbon concentration as well as determination of their intracellular carbon content. As these biogeochemical quantities cannot be acquired automatically and are therefore impossible to sample from a mooring, new methods have to be considered. Recent technological advances now make it possible to perform automated in situ investigations of phytoplankton composition (using imaging-in-flow cytometry, Sosik and Olson 2007) and particle size distribution (using the laser in situ scattering and transmissometry, Reynolds et al. 2010). The next generation of ocean observatories could combine these approaches to better understand the diel dynamics of particle assemblages.

Acknowledgments

We thank Hervé Claustre, Antoine Sciandra, Dariusz Stramski, and Rick Reynolds for their excellent suggestions on earlier versions on this paper. We are grateful to Emmanuel Boss and one anonymous reviewer for constructive criticism on the initial version of the manuscript.

P.G. benefited from a grant provided by the ACRI-st company and the French National Association for Research and Technology. The Bouée pour l'acquisition de Séries Optiques à Long Terme (BOUSSOLE) project is supported and funded by the Centre National de la Recherche Scientifique, the Institut National des Sciences de l'Univers, the French space agency Centre National d'Etudes Spatiales, the European Space Agency, and the National Aeronautics and Space Administration of the United States through a Letter of Agreement with the Université Pierre et Marie Curie.

References

Andersen, V., M. Goutx, L. Prieur, and J. R. Dolan. 2009. Short-scale temporal variability of physical, biological and biogeochemical processes in the NW Mediterranean Sea: An introduction. Biogeosciences **6:** 453–461, doi:10.5194/bg-6-453-2009

Antoine, D., and A. Morel. 1996. Oceanic primary production 1. Adaptation of a spectral light-photosynthesis model in view of application to satellite chlorophyll observations. Global Biogeochem. Cycles **10:** 43–55, doi:10.1029/95GB02831

———, F. D'Ortenzio, S. B. Hooker, G. Bécu, B. Gentili, D. Tailliez, and A. Scott. 2008. Assessment of uncertainty in the ocean reflectance determined by three satellite ocean color sensors (MERIS, SeaWiFS and MODIS-A) at an offshore site in the Mediterranean Sea (BOUSSOLE project). J. Geophys. Res. **113:** C07013, doi:10.1029/2007JC004472

———, and others. 2006. BOUSSOLE: A Joint CNRS-INSU, ESA, CNES and NASA ocean color calibration and validation activity. NASA Tech. Memo. 2006-214147.

Babin, M., A. Morel, H. Claustre, A. Bricaud, Z. Kolber, and P. G. Falkowski. 1996. Nitrogen- and irradiance-dependent variations of the maximum quantum yield of carbon fixation in eutrophic, mesotrophic and oligotrophic marine systems. Deep-Sea Res. I **43:** 1241–1272, doi:10.1016/0967-0637(96)00058-1

Behrenfeld, M. J. 2010. Abandoning Sverdrup's critical depth hypothesis on phytoplankton blooms. Ecology **91:** 977–989, doi:10.1890/09-1207.1

———, and E. Boss. 2003. The beam attenuation to chlorophyll ratio: An optical index of phytoplankton physiology in the surface ocean? Deep-Sea Res. I **50:** 1537–1549, doi:10.1016/j.dsr.2003.09.002

Bishop, J. K. B. 1986. The correction and suspended particulate matter calibration of SeaTech transmissiometer data. Deep-Sea Res. **33:** 121–134.

———, S. E. Calvert, and M. Y. S. Soon. 1999. Spatial and temporal variability of POC in the northeast subarctic Pacific. Deep-Sea Res. II **46:** 2699–2733, doi:10.1016/S0967-0645(99)00081-8

———, R. E. Davis, and J. T. Sherman. 2002. Robotic observations of dust storm enhancement of carbon biomass in the North Pacific. Science **298:** 817–821, doi:10.1126/science.1074961

Boss, E., W. H. Slade, M. Behrenfeld, and G. Dall'Olmo. 2009. Acceptance angle effects on the beam attenuation in the ocean. Opt. Express **17:** 1535–1550, doi:10.1364/OE.17.001535

Bricaud, A., A. Morel, and L. Prieur. 1981. Absorption by dissolved organic matter of the sea (yellow substance) in the UV and visible domains. Limnol. Oceanogr. **26:** 43–53, doi:10.4319/lo.1981.26.1.0043

Bruyant, F., and others. 2005. Diel variations in the photosynthetic parameters of *Prochlorococcus* strain PCC 9511: Combined effects of light and cell cycle. Limnol. Oceanogr. **50:** 850–863, doi:10.4319/lo.2005.50.3.0850

Byrd, R. H., P. Lu, J. Nocedal, and C. Zhu. 1995. A limited memory algorithm for bound constrained optimization. SIAM J. Sci. Comput. **16:** 1190–1208, doi:10.1137/0916069

Church, M. J., H. W. Ducklow, and D. M. Karl. 2004. Light dependence of [^{3}H] leucine incorporation in the oligotrophic North Pacific Ocean. Appl. Environ. Microbiol. **70:** 4079–4087, doi:10.1128/AEM.70.7.4079-4087.2004

Claustre, H., Y. Huot, I. Obernosterer, B. Gentili, D. Tailliez, and M. Lewis. 2007. Gross community production and metabolic balance in the South Pacific Gyre, using a nonintrusive bio-optical method. Biogeosciences **5:** 463–474, doi:10.5194/bg-5-463-2008

———, and others. 1999. Variability in particle attenuation and chlorophyll fluorescence in the tropical Pacific: Scales, patterns, and biogeochemical implications. J. Geophys. Res. **104:** 3401–3422, doi:10.1029/98JC01334

———, and ———. 2002. Diel variations in *Prochlorococcus* optical properties. Limnol. Oceanogr. **47:** 1637–1647, doi:10.4319/lo.2002.47.6.1637

Cullen, J. J., M. Lewis, C. O. Davis, and R. Barber. 1992. Photosynthetic characteristics and estimated growth rates indicate grazing is the proximate control of primary production in the Equatorial Pacific. J. Geophys. Res. **97:** 639–655, doi:10.1029/91JC01320

D'Asaro, E. 2008. Convection and the seeding of the North Atlantic bloom. J. Mar. Sys. **69:** 233–237, doi:10.1016/j.jmarsys.2005.08.005

D'Ortenzio, F., and others. 2005. Seasonal variability of the mixed layer depth in the Mediterranean Sea as derived from in situ profiles. Geophys. Res. Lett. **32:** L12605, doi:10.1029/2005GL022463

Doty, M. S., and M. Oguri. 1957. Evidence for a photosynthetic daily periodicity. Limnol. Oceanogr. **2:** 37–40, doi:10.4319/lo.1957.2.1.0037

Durand, M. D., and R. J. Olson. 1996. Contributions of phytoplankton light scattering and cell concentration changes to diel variations in beam attenuation in the equatorial Pacific from flow cytometric measurements of pico-, ultra- and nanoplankton. Deep-Sea Res. II **43:** 891–906, doi:10.1016/0967-0645(96)00020-3

Fuhrman, J. A., R. W. Eppley, A. Hagström, and F. Azam. 1985. Diel variations in bacterioplankton, phytoplankton, and related parameters in the Southern California Bight. Mar. Ecol. Prog. Ser. **27:** 9–20, doi:10.3354/meps027009

Gardner, W. D., S. P. Chung, M. J. Richardson, and I. D. Walsh. 1995. The oceanic mixed-layer pump. Deep-Sea Res. **42:** 757–775, doi:10.1016/0967-0645(95)00037-Q

———, J. S. Gundersen, M. J. Richardson, and I. D. Walsh. 1999. The role of seasonal and diel changes in mixed-layer depth on carbon and chlorophyll distributions in the Arabian Sea. Deep-Sea Res. II **46:** 1833–1858, doi:10.1016/S0967-0645(99)00046-6

———, A. V. Mishonov, and M. J. Richardson. 2006. Global POC concentrations from in-situ and satellite data. Deep-Sea Res. II **53:** 718–740, doi:10.1016/j.dsr2.2006.01.029

———, I. D. Walsh, and M. J. Richardson. 1993. Biophysical forcing of particle production and distribution during a spring bloom in the North Atlantic. Deep-Sea Res. II **40:** 171–195, doi:10.1016/0967-0645(93)90012-C

Gasol, J. M., M. D. Doval, J. Pinhassi, J. Calderón-Paz, N. Guixa-Boixareu, D. Vaqué, and C. Pedrós-Alió. 1998. Diel variations in bacterial heterotrophic activity and growth in the northwestern Mediterranean Sea. Mar. Ecol. Prog. Ser. **164:** 107–124, doi:10.3354/meps164107

Gernez, P. 2009. Analyse de la variabilité temporelle des propriétés optiques en mer Ligure depuis un mouillage instrumenté (site Boussole): Fluctuations à haute fréquence, cyclicité diurne, changements saisonniers et variabilité interannuelle. Ph. D. thesis. Université Pierre et Marie Curie. [Temporal variability of optical properties in the Ligurian Sea from an instrumented mooring: Analysis of high-frequency fluctuations, diel cycles, seasonal and interannual changes.]

Harding, L. W., B. W. Meeson, B. B. Prézelin, and B. M. Sweeney. 1981. Diel periodicity of photosynthesis in marine phytoplankton. Mar. Biol. **61:** 95–105, doi:10.1007/BF00386649

———, B. B. Prézelin, B. M. Sweeney, and J. L. Cox. 1982. Primary production as influenced by diel periodicity of phytoplankton photosynthesis. Mar. Biol. **67:** 179–186, doi:10.1007/BF00401283

Ikushima, I. 1967. Ecological studies on the productivity of aquatic plant communities. III. Effect of depth on daily photosynthesis in submerged macrophyte. Bot. Mag. **80:** 57–67.

Jassby, A. D., and T. Platt. 1976. Mathematical formulation of the relationship between photosynthesis and light for phytoplankton. Limnol. Oceanogr. **21:** 540–547, doi:10.4319/lo.1976.21.4.0540

Kiefer, D. A. 1973. Fluorescence properties of natural phytoplankton populations. Mar. Biol. **22:** 263–269, doi:10.1007/BF00389180

Kinkade, C. S., J. Marra, T. D. Dickey, C. Langdon, D. E. Sigurdson, and R. Weller. 1999. Diel bio-optical variability observed from moored sensors in the Arabian Sea. Deep-Sea Res. II **46:** 1813–1831, doi:10.1016/S0967-0645(99)00045-4

Kitchen, J. C., and J. R. V. Zaneveld. 1990. On the noncorrelation of the vertical structure of light scattering and chlorophyll *a* in case 1 waters. J. Geophys. Res. **95:** 20237–20246, doi:10.1029/JC095iC11p20237

Loisel, H., and A. Morel. 1998. Light scattering and chlorophyll concentration in case 1 waters: A reexamination. Limnol. Oceanogr. **43:** 847–858, doi:10.4319/lo.1998.43.5.0847

Malone, T. C. 1971. Diurnal rhythms in netplankton and nannoplankton assimilation ratios. Mar. Biol. **10:** 285–289, doi:10.1007/BF00368086

Marra, J. 1997. Analysis of diel variability in chlorophyll fluorescence. J. Mar. Res. **55:** 767–784, doi:10.1357/0022240973224274

———. 2002. Approaches to the measurement of plankton production, p. 78–108. *In* P. J. le B. Williams, D. N. Thomas, and C. S. Reynolds [eds.], Phytoplankton productivity: Carbon assimilation in marine and freshwater ecosystems. Blackwell.

Marty, J.-C., and J. Chiaverini. 2002. Seasonal and interannual variations in phytoplankton production at DYFAMED time-series station, northwestern Mediterranean Sea. Deep-Sea Res. II **49:** 2017–2030, doi:10.1016/S0967-0645(02)00025-5

———, ———, M. D. Pizay, and B. Avril. 2002. Seasonal and interannual dynamics of nutrients and phytoplankton pigments in the western Mediterranean Sea at the DYFAMED time-series station (1991–1999). Deep-Sea Res. II **49:** 1965–1985, doi:10.1016/S0967-0645(02)00022-X

———, N. Garcia, and P. Raimbault. 2008. Phytoplankton dynamics and primary production under late summer conditions in the NW Mediterranean Sea. Deep-Sea Res. **155:** 1131–1149.

Mével, G., M. Vernet, M. Goutz, and J. F. Ghiglione. 2008. Seasonal to hour variation scales in abundance and production of total and particle-attached bacteria in the open NW Mediterranean Sea (0–1000 m). Biogeosciences **5:** 1573–1586, doi:10.5194/bg-5-1573-2008

Millot, C. 1999. Circulation in the western Mediterranean Sea. J. Mar. Sys. **20:** 423–442, doi:10.1016/S0924-7963(98)00078-5

Montes-Hugo, M. A., H. Ducklow, and O. M. Schofield. 2009. Contribution by different marine bacterial communities to particulate beam attenuation. Mar. Ecol. Prog. Ser. **379:** 13–22, doi:10.3354/meps07883

Morel, A. 1991. Light and marine photosynthesis: A spectral model with geochemical and climatological implications. Prog. Oceanogr. **26:** 263–306, doi:10.1016/0079-6611(91)90004-6

———, and J.-F. Berthon. 1989. Surface pigments, algal biomass profiles, and potential production of the euphotic layer: Relationships reinvestigated in view of remote-sensing applications. Limnol. Oceanogr. **34:** 1545–1562, doi:10.4319/lo.1989.34.8.1545

———, and A. Bricaud. 1986. Inherent optical properties of algal cells including phytoplankton: Theoretical and experimental results. Can. Bull. Fish. Aquat. Sci. **214:** 521–559.

———, and L. Prieur. 1977. Analysis of variations in ocean color. Limnol. Oceanogr. **22:** 709–722, doi:10.4319/lo.1977.22.4.0709

Ondrusek, M. E., R. R. Bidigare, K. Waters, and D. M. Karl. 2001. A predictive model for estimating rates of primary production in the subtropical North Pacific Ocean. Deep-Sea Res. II **48:** 1837–1863, doi:10.1016/S0967-0645(00)00163-6

Oubelkheir, K. 2001. Caractérisation biogéochimique de provinces océaniques à l'aide d'indicateurs bio-optiques, à diverses échelles spatio-temporelles. Ph. D. thesis. Université de la Méditerranée. [Biogeochemical characterization of oceanic provinces using bio-optical indexes, at various spatiotemporal scales.]

———, H. Claustre, A. Sciandra, and M. Babin. 2005. Bio-optical and biogeochemical properties of different trophic regimes in oceanic waters. Limnol. Oceanogr. **50:** 1795–1809, doi:10.4319/lo.2005.50.6.1795

———, AND A. SCIANDRA. 2008. Diel variations in particle stocks in the oligotrophic waters of the Ionian Sea (Mediterranean). J. Mar. Sys. **74:** 364–371, doi:10.1016/j.jmarsys.2008.02.008

RAS, J., J. UITZ, AND H. CLAUSTRE. 2008. Spatial variability of phytoplankton pigment distributions in the subtropical South Pacific Ocean: Comparison between in situ and modeled data. Biogeosciences **5:** 353–369, doi:10.5194/bg-5-353-2008

REYNOLDS, R. A., D. STRAMSKI, V. M. WRIGHT, AND S. B. WOŹNIAK. 2010. Measurements and characterization of particle size distributions in coastal waters. J. Geophys. Res. **115:** C08024, doi:10.1029/2009JC005930

RYTHER, J. H., AND C. S. YENTSCH. 1957. The estimation of phytoplankton production in the ocean from chlorophyll and light data. Limnol Oceanogr. **2:** 281–286.

SHIMADA, B. M. 1958. Diurnal fluctuations in photosynthetic rate and chlorophyll *a* content of phytoplankton from eastern Pacific waters. Limnol. Oceanogr. **3:** 336–339, doi:10.4319/lo.1958.3.3.0336

SIEGEL, D. A., T. D. DICKEY, L. WASHBURN, M. K. HAMILTON, AND B. G. MITCHELL. 1989. Optical determination of particulate abundance and production variations in the oligotrophic ocean. Deep-Sea Res. **36:** 211–222.

SOSIK, H. M., AND R. J. OSLON. 2007. Automated taxonomic classification of phytoplankton sampled with imaging-in-flow cytometry. Limnol. Oceanogr. Methods **5:** 204–216.

SOURNIA, A. 1974. Circadian periodicities in marine populations of phytoplankton. Adv. Mar. Biol. **12:** 325–389, doi:10.1016/S0065-2881(08)60460-5

STRAMSKA, M., AND T. D. DICKEY. 1992. Variability of bio-optical properties of the upper ocean associated with diel cycles in phytoplankton population. J. Geophys. Res. **97:** 17873–17887, doi:10.1029/92JC01570

———, ———, A. PLUEDDEMANN, R. WELLER, C. LANGDON, AND J. MARRA. 1995. Bio-optical variability associated with phytoplankton dynamics in the North Atlantic Ocean during spring and summer of 1991. J. Geophys. Res. **100:** 6621–6632, doi:10.1029/94JC01447

STRAMSKI, D., AND D. A. KIEFER. 1991. Light scattering by microorganims in the open ocean. Prog. Oceanogr. **28:** 343–383, doi:10.1016/0079-6611(91)90032-H

———, AND R. A. REYNOLDS. 1993. Diel variations in the optical properties of a marine diatom. Limnol. Oceanogr. **38:** 1347–1364, doi:10.4319/lo.1993.38.7.1347

TAGUCHI, S. 1976. Short-term variability of photosynthesis in natural marine phytoplankton populations. Mar. Biol. **37:** 197–207, doi:10.1007/BF00387604

UITZ, J., H. CLAUSTRE, A. MOREL, AND S. B. HOOKER. 2006. Vertical distribution of phytoplankton communities in open ocean: An assessment based on surface chlorophyll, J. Geophys. Res. **111:** C08005, doi:10.1029/2005JC003207

VAN WAMBEKE, F., M. TEDETTI, S. DUHAMEL, AND R. SEMPÉRÉ. 2009. Diel variability of heterotrophic bacterial production and underwater UV doses in the eastern South Pacific. Mar. Ecol. Prog. Ser. **387:** 97–108, doi:10.3354/meps08075

WALSH, I. D., S. P. CHUNG, M. J. RICHARDSON, AND W. D. GARDNER. 1995. The diel cycle in the integrated particle load in the equatorial Pacific: A comparison with primary production. Deep-Sea Res. II **42:** 465–477, doi:10.1016/0967-0645(95)00030-T

Associate editor: Heidi M. Sosik

Received: 24 February 2010
Accepted: 16 September 2010
Amended: 20 September 2010